Progress in Polymer Science 38 (2013) 963–991

Contents lists available at SciVerse ScienceDirect

Progress in Polymer Science

journal homepage: www.elsevier.com/locate/ppolysci

Functional materials by electrospinning of polymers

Seema Agarwal[a], Andreas Greiner[a], Joachim H. Wendorff[b,*]

[a] Lehrstuhl für Makromolekulare Chemie II, Bayreuth Center for Colloids and Interfaces (BZKG), Gebäude NWII, Universität Bayreuth, Universitätsstrasse 30, 95440 Bayreuth, Germany

[b] Philipps-Universität Marburg, Department of Chemistry and Scientific Center for Materials Science, Hans-Meerwein Straße, D-35032, Germany

ARTICLE INFO

Article history:
Received 31 July 2012
Received in revised form 24 January 2013
Accepted 24 January 2013
Available online 6 February 2013

Keywords:
Electrospinning
Functional nanofibers
Magnetic properties
Optoelectronic applications

ABSTRACT

About a decade ago electrospinning was primarily concerned with the preparation of nanofibers from synthetic polymers and to a lower degree from natural polymers targeting predominantly technical applications areas such as textiles and filters as well as medical areas such as tissue engineering and drug delivery. Since then strong progress has been made not only in the understanding and theoretical modeling of the complex processes governing electrospinning and in the strict control of fiber formation by material and operating parameters but also in the design of a broad range of technical spinning devices. These achievements have in turn allowed for an extension of electrospinning towards fiber formation based not only on polymers – of synthetic, biological nature – but also on metals, metal oxides, ceramics, organic/organic, organic/inorganic as well as inorganic/inorganic composite systems. Here not only preparation schemes were investigated but properties and functions of the nanofibers were analyzed and potential applications were evaluated. As far as technical applications are concerned nanofibers composed of such materials can today be designed in a highly controlled way to display specific structural features. They include phase morphology and surface topology as well as unique functions including in particular magnetic, optical, electronic, sensoric, catalytic functions specific for one-dimensional architectures. Significant developments have also been achieved towards the exploitation of such functional nanofibers in applications involving among others fuel cells, lithium ion batteries, solar cell, electronic sensors as well as photocatalysts. One major target is currently the incorporation of such functional nanofibers in micrometer-sized electronic devices or even the construction of such devices purely from nanofibers.

Contents

* Corresponding author. Tel.: +49 6421 2825777; fax: +49 6421 2825785.
E-mail address: wendorff@staff.uni-marburg.de (J.H. Wendorff).

0079-6700/$ – see front matter © 2013 Elsevier Ltd. All rights reserved.
http://dx.doi.org/10.1016/j.progpolymsci.2013.02.001

1. Introduction

Within the last decade electrospinning of polymers has become an internationally highly recognized method for the preparation of polymer nanofibers with diameters down to a few nanometers and of a broad range of complex architectures of nanofibers and nonwovens [1–7]. This is obvious from the ever growing number of papers published amounting currently to 2000 publications per year. These papers reflect significant progress which has been made in a variety of topics within the last years. Such topics include (a) the understanding and modeling of the complex processes governing electrospinning, (b) the control of fiber formation by material and operating parameters, (c) improvements and multiple extensions made to technical spinning devices and (d) the extension of electrospinning towards fiber formation based not only on polymers – of synthetic, natural, biological nature – but also on metals, metal oxides, ceramics, organic/organic, organic/inorganic as well as inorganic/inorganic composite systems. Here not only preparation schemes were investigated but properties and functions of the nanofibers were also evaluated and potential applications discussed.

Such applications include medical areas such as tissue engineering and drug delivery not discussed in this paper in view of existing reviews [8–10] as well as technical areas relying on nanofibers with specific photonic, electronic, photocatalytic and magnetic properties. Fuel cells, lithium ion batteries, solar cells, electronic sensors, energy storage systems are assumed to benefit strongly from nanofiber-based architectures. It is frequently pointed out in corresponding papers that key features which make nanofibers and nonwovens of interest for such types of applications are the 1D-confinements characteristic of nanofibers, the high orientations of structural elements induced along the fibers via electrospinning, strongly restricted material and electronic diffusion distances perpendicular to the fiber axis, high surface area as well as the high porosities of up to 90% observed for electrospun nonwovens. Substantial progress has, of course, also been made in a range of other areas including textile applications, filter applications, fiber reinforcement and many more [11–14]. Yet in view of the more than 10,000 papers published within the last decade and the correspondingly large number of issues treated in them a selection of specific topics to be addressed in this review had to be made.

2. The electrospinning system

2.1. Understanding and modeling the complex processes governing electrospinning

Of general importance is the recognition that fiber formation processes in electrospinning differ fundamentally from the ones in conventional technical approaches which rely predominantly on mechanical forces and geometric boundary conditions. Such conventional techniques include extrusion with in general follow-up elongations, melt blowing or techniques based on converging flow. In contrast, fiber formation in electrospinning is governed by self-assembly processes as induced by electric charges. All the key features characteristic of the spinning process including not only the evolution of the final diameter of the nanofibers in electrospinning but also undulations of the fiber diameter, the formation of beaded structures with droplets located along the fibers in a regular fashion can be attributed to the presence of repulsive Coulomb interactions between charged elements of the fluid jet. Self assembly happens according to the general Earnshaw theorem of electrostatics. It states that it is impossible to prepare stable fluid structures such as, for instance, stable fluid jets in which all elements interact only by Coulomb forces [15,16]. Charges within the fluid jet subject the charged polymer elements to motions along complex pathways so that the Coulomb interaction energy becomes minimized. Self-assembly processes in electrospinning take place not only in simple fibers but also in fibers of complex shapes such as flat fibers, in fibers with vertical protrusions, splayed fibers. Detailed theoretical [16–25] as well as experimental investigations [26–55] on the nature of the processes governing fiber formation have advanced electrospinning significantly in the last decade. Identified were as key processes (1) droplet deformation at the feeding units/tip of die, onset of jetting, (2) development of a rectilinear jet, (3) onset of bending deformations with looping, spiralling trajectories, (4) deposition on counter electrodes/substrates. Yet additional processes also exist which affect fiber geometries considerably including the Rayleigh type instability, the

electrically driven axisymmetric instability and branching processes. These processes have been characterized experimentally and modeled in detail [16–55].

As far as the initial step towards fiber formation in electrospinning is concerned the formation of electrically charged droplets composed of the spinning solution or melt at the primary electrode, the shape of the droplets, their stability in the electric field as well as the onset of jetting were experimentally and theoretically analyzed in detail by G.H. Reneker and A.L. Yarin as primary investigators [16–21]. For fluid droplets in the electric field the observation is that such a droplet becomes more and more prolate extending in the direction of the field as the electric field is increased. These prolate shapes correspond to equilibrium states as controlled predominantly by the balance between the electric and surface forces. As the strength of the electric field is increased even further approaching a critical value E^* the fluid droplet assumes a cone like shape with a characteristic half angle of the cone of the order of 30° and above. A further increase of the field causes the droplet to become unstable and a fluid jet emanates from the tip of the droplet. A more detailed analysis of this situation has revealed two interesting features [24]. The first concerns the flow pattern around the jet in the cone region. Using a tracer technique it has become obvious that a strong flow takes place which is directed towards the apex of the surface of the cone while a weaker backflow occurs towards the centre line of the cone. This circulation of the fluid has been attributed to the presence of tangential electrical shear stresses. The second feature is that the cone becomes more concave close to the tip while the cone shape tends to vanish at still larger fields either because it has been shifted into the die or because of strong circulations which remove the fluid from the droplet [24].

In the theoretical analysis of droplet shape in electric fields [5,17,19] it was assumed that a hyperboloid of revolution should be a reasonably good representation of the shape of the droplet. The analysis predicts that a critical hyperboloid is stable for the maximum potential for which a stationary shape can exist with an envelope cone displaying a half angle of 33.5°. This is, in fact, close to the experimentally observed values. A further result is that the distance over which the distortions of the electric field induced by the cone-shaped charged droplet take place is surprisingly small amounting to only about 1 μm. Finally the radius of curvature at the tip of the hyperboloid of rotation at a potential corresponding to the onset of instability, i.e. to the onset of jetting, is of the order of 10^{-1} μm. This is very small compared to the diameter, for instance, of the syringe-type dies used in many spinning set-ups.

The jets emerging from the tip of the cone-shaped droplets are observed to move towards the counter electrode in a linear straight fashion for some distance. The jet diameter decreases along its trajectory typically by a factor of about 4 over a distance of 10 cm which corresponds to the reduction of the cross section by a factor of about 20 [5,17]. A significant part of this decrease comes from the evaporation of the solvents yet a further contribution originates from longitudinally deformations of the jet induced by electric forces. Tracer particle tracking techniques involving high speed photography have revealed that elements of the fluid jet are subjected to accelerations of up to 600 m/s^2. These are thus two orders of magnitude larger then the acceleration coming from gravitational forces, i.e. the conclusion is that gravitational forces play no significant role in electrospinning. The velocity of fluid elements within the jets amounts to only a few cm/s very close to the beginning of the emerging jet. Yet it increases to up to several m/s at a jet length in the range of 1 cm and above [5,17]. Further characteristic values coming from the analysis of the particle tracking techniques are strain rates approaching values of the order of 1000 s^{-1} and elongational deformations of up to 1000. The strain rates characteristic for the straight part of the jet are consequently large enough to induce chain extension.

To account for a limited length of the straight part of the jet the assumption that has been made is that no deviations occur as long as the conditions are such that no instabilities, in particular the bending instability, can become dominant. The concept theoretically explored is that such bending instabilities can become dominant only if the total tensile stress has decayed sufficiently along the jet. Yarin and Reneker have considered in this context a rather simple model for calculating thus the length of the linear path of the jet and the onset of instabilities [5,16]. Modeled is the linear segment of the jet in terms of a viscoelastic dumbbell. The predictions are that the stress/longitudinal force first increases over time as the segment is stretched, passes a maximum as function of time and then begins to decrease. The decrease is attributed to the onset of the visco-elastic relaxation process characteristic of the Maxwell model. The interpretation proposed is as follows. The linear jet is stable for sufficiently high values of force and stress. Yet as these pass through a maximum and decay rather strongly at larger times i.e. at locations further down the jet they become so small that instabilities, in particular the bending instability, become dominant. This causes the linear jet to deviate from the original path at a length which is strongly controlled by the applied voltage in agreement with experimental findings. This characteristic length is interpreted as the length of the linear part of the jet observed experimentally.

Beyond this length the jet is subjected to bending deformations i.e. it deviates thus from straight path directed towards the counter electrode. It turns sideways and displays spiralling, looping motions [5,16,21]. In each loop the jet decreases in diameter and becomes elongated while the loop diameters increases strongly. The envelope of these loops resembles a cone with its opening oriented towards the counter electrode. This type of instability – called bending but frequently also whipping instability – repeats itself on a smaller and smaller scale obviously in a self-similar fashion as the jet diameter is reduced. The overall draw ratio is found to be of the order of 10^5 and the overall strain rate approaches 10^5 s^{-1} [5,21]. To represent this type of instability the jet was modeled via a chain of beads with given charge and mass connected by viscoelastic elements as used already above for the analysis of the linear part of the jet [5,16]. Both space and time dependent perturbations of the jet causes within the framework of the model the development of electrically driven bending instabilities. The predicted jet trajectory resembles the experimentally

observed bending trajectory of the jet closely in that it provides a reasonably accurate description of the path of the jet including the complex looping and spiraling motions. This holds for the conic envelop of the path within the bending instability range and also for the magnitudes of the diameter reduction, total elongation and deformation rate which the jet experiences [5,16].

The deposition of solidified nanofibers onto the counter electrode or substrates located on top of the counter electrode is the final step in electrospinning. One key topic in this context is the velocity of the fiber formation and deposition process. One argument based on the consideration of the reduction of the cross sectional area of the jet in electrospinning (including solvent evaporation) is that a corresponding rectilinear elongation would result in a velocity of the fiber end with an unrealistic magnitude amounting to more than 100 times the speed of sound. Yet the treatment of the bending instability [5,16] reveals that most of the elongation takes place in the loops of the bending motions causing the downward velocity of the loops to be much smaller. The corresponding velocity is of the order of just 1 m/s. The transverse velocity of a given loop tends to be of the order of several 10 m/s.

As far as the geometry of the deposition pattern is concerned it is controlled by the geometry of the envelope cone i.e. the conic angle characteristic of the envelope of the path of the jet subjected to bending instabilities as well as by the distance between the onset of the bending instability and the deposition on a substrate. Investigations have shown that the conic angle of the envelope is a characteristic feature of the complex electrospinning process. It depends significantly on spinning parameters such as the applied voltage, the polymer concentration in the spinning solution, the feeding rate of the spinning solution but also the diameter of the nozzle [26]. The observation for model spinning solutions composed of poly(acrylonitrile) (PAN) and dimethylformamide is that the conic angle can be varied between about 35° up to about 165° depending on the choice of the absolute magnitude of these parameters. The strongest effect comes from the electric field causing the conic angle to increase from 35° to 165° as the field is increased from 50 to 100 kV/m, for instance. An increase of the feeding rate from 0.4 to 1 ml/h causes the conic angle to increase from about 95° to about 155° and an increase of the polymer concentration from 12 to 20 wt% leads to a reduction of the conic angle from about 165° to about 70°. Finally a smaller nozzle diameter has been found to cause a smaller increase of the conic angle with the applied field compared to larger nozzle diameter. Interpretations are that larger applied fields cause stronger electrostatic repulsions between the bending loops, increased polymer concentrations cause the loop stretching to slow down because of larger viscosities. As far as the effect of the feeding rate is concerned the interpretation is that larger feeding rates cause larger droplets at the nozzle outlet which alters the Taylor cone and jet initiation [26].

In electrospinning in addition to linear fibers frequently fibers with spindle type beads or beads approaching a spherical shape along the fibers have been observed [4,5,7]. Such structures were attributed to the presence of instabilities other than the bending instability including the Rayleigh instability and an axisymmetric instability. Their effect on fiber formation has been investigated in detail in a set of theoretical approaches with Brenner and Rutledge as primary investigators [22–24]. The theoretical analysis relies on classical hydrodynamics focusing on charged fluid cylindrical elements – representing the jet in electrospinning – located in an electric field. Predicted are operating diagrams for electrospinning in terms of the feeding rate of the spinning solution and the applied electrical field for given properties of the spinning fluids. Such diagrams specify electrospinning parameter sets for which bending can be expected. Yet they also indicate parameters for which other types of instabilities dominate yielding, for instance, fibers droplets.

In addition branching effects to which the jet is subjected during the spinning process have been observed depending on the spinning parameters chosen. Frequently a branch has been found to occur along the path of the jet in an isolated fashion but for other conditions a regular arrangement of such branches along the jet path has been reported [20]. The length of the branches which emerge may be rather limited but frequently these branches grow in length also becoming quickly thinner and thinner. These branches will not only be observed for the jet but also for the final solid fibers as deposited on the counter electrode/substrate. Theoretical investigations have revealed that branching originates definitely from electric effects, has no counterpart in extrusion fiber spinning and the distribution of the branches along the fibers can be successfully modeled [20]. In fact, fibers can be produced via branching effects characterized by a regular arrangement of geometrically well defined barbs [27].

In conclusion, the theoretical analysis both of the individual physical processes characteristic of electrospinning as well as their complex superposition controlling fiber formation has been advanced remarkably. Reliable guidelines have thus been developed which allow the design and optimization of nanofiber production routes to a considerable extent particularly as far as single die configurations are concerned. A need for further and more detailed modeling activities exists in the area of novel more recently developed spinning configurations including those characteristic of bubble spinning, gas-jet electrospinning, conical wire coil spinning.

2.2. *Effects of material and operating parameters on fiber formation*

The range of parameters known to affect electrospinning of nanofibers and corresponding nonwovens which have been considered in the literature within the last decade is extremely broad as obvious already from a set of review articles [1–7]. Considered was the control of fiber diameters, of fiber formation with ribbon- like shapes, of the onset of beading, of the formation of porous fibers, of the production of fibers with branches, and of the magnitude of the angle of the conic envelope of the bending path affecting the deposition pattern. In the following the current state will be briefly reported for specific spinning parameters.

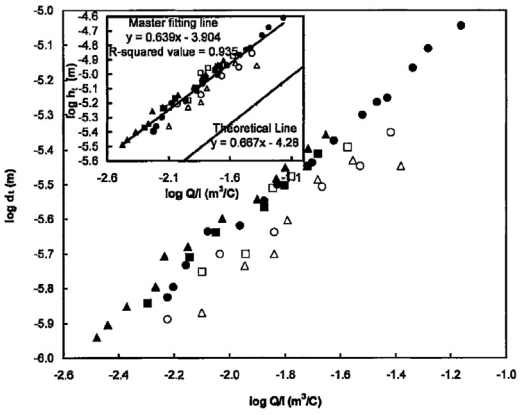

Fig. 1. Log of the fiber diameter d_t plotted versus log Q/I, corresponding master lines for the terminal jet diameter are given in the insert. Reprinted with permission from ref. [25]. Copyright (2003) The American Physical Society.

A decrease of the orifice size has been found to decrease fiber diameters [28]. The effect of the collector distance on fiber diameters has been considered in a set of investigations [29–36]. A decrease of the diameter with increasing collector distances results as far as smooth fibers are concerned [31] yet for beaded fibers beads tend to grow with increasing collector distance. Increasing flow rates are reported to increase fiber diameters and bead diameters [30–33,37–41] yet it has been pointed out that such effects may often be interrelated with effects coming from volumetric charge density effects. The volumetric charge density also seems to affect the morphology of the fibers including bead formation [37]. The feeding rate as a key parameter in controlling the diameter of the final fibers has been evaluated also theoretically using a model for stretching of a viscous charged fluid in an electric field [25]. The prediction is that it is the balance between surface tension and charge repulsion contributions which controls the final diameter h_t of the jet according to:

$$h_t \sim \left(\frac{Q}{I}\right)^{2/3} \gamma^{1/3}$$

with Q being the flow rate, I the electric current characteristic of the spinning experiment and γ the surface tension of the fluid. Taking the evaporation of the solvent during fiber formation into account (concentration c) the fiber diameter d_t results as follows

$$d_t = c^{1/2} h_t$$

Fig. 1 shows corresponding experimental results for polycaprolactone (PCL) solutions where the log of the fiber diameter d_t is plotted versus log $(I/Q)^{-1}$. These are in line with the theoretical predictions [41].

Since surface tension and the conductivity of polymer solutions and thus the current in electrospinning are determined primarily by the solvent, the flow rate turns out to be a primary control parameter for the fiber diameter. This diameter is predicted to increase with the flow rate – in agreement with experimental findings – following a power law. Considering viscosity as parameter one observation is that the fiber morphology depends strongly on the viscosity of the spinning solution [29,34]. Also, the fiber diameters will increase if the zero-shear viscosity is increased via higher polymer concentrations or also via the use of polymers of higher molecular weight in the spinning solution. The initial polymer concentrations of the spinning solutions – tending to be in the range from 1 about 30 wt% with 40 wt% also being used in specific cases – is a spinning parameter considered in various papers [29–35,42]. Unfortunatelly in most papers initial concentrations are varied without ensuring that the values for all other variables remain constant. Ref. [36] states that the diameters of Nylon-6 fibers increase from 80 to 230 nm if the initial polymer concentration is increased from 10 to 25 w%. A set of papers considers the effect of various solvents on the electrospinning process with vapour pressure being one target parameter [31,32,40,41,43,44]. However, the morphological changes may also result from conductivity, viscosity or surface tension effects. In any case low vapor pressure solvents tend to enhance nozzle plugging if no sufficient flow can be induced. Papers on electrospinning considering solution densities [31,42,45] point out that the values were very close to the corresponding pure solvents (within 5%).

Progress has definitely been made more recently in recognizing the importance of the quality of a solvent in controlling electrospinning. In the case of electrospinning of polyamides from formic acid as good solvent it was, for instance, observed that the stability of the spinning process and the quality of the fibers could be improved considerably if various amounts of the nonsolvent acetic acid were added to the spinning solution. On a qualitative level the quality of a solvent has been judged on the time it took to dissolve the given polymer to form a homogeneous solution yielding categories such as poor, partial, partial to high, and high solubilities [46]. Detailed information on the impact of the quality of solvents on electrospinning has come from systematic studies considering model systems comprising 28 different solvents as well as mixtures of them with poly (methylsilesquioxane) (PMSQ), a nonpolar biocompatible polymer [46]. The experimental finding was as far as single component solvents are concerned that good solvents tend to give rise to electrospraying whereas partial solubility systems give rise to stable electrospinning of fibers while with poor solvents no spinning could be induced at all. Along the same direction binary solvent systems were analyzed with respect to their impact on electrospinning. Solubility parameters were used furthermore to put the results on a more quantitative level and spinnability–solubility maps were constructed allowing for a systematic selection of solvents/solvent pairs for electrospinning [46]. Based on these investigations it is suggested that lower solubility can be better suited for making good electrospinning solutions than solvents of high solubility.

Investigations on the effect of the conductivity of the solutions on electrospinning particulary due to the presence or absence of salts have revealed the significant importance of this parameter [47–49]. One result is that an increase of the conductivity tends to suppress the formation of beads [49]. Furthermore for the case of poly(acrylonitrile) (PAN) solutions the observation is that

no fiber can be produced by electrospinning either for highly insulating solution or for applied voltage not high enough. Such problems could be overcome if salts are added to the spinning solution [47]. Considering effects coming from variations of the electric potential for poly (lactide-co-glycolide) (PLAGA) fibers a decrease of their diameter from 900 to 450 nm is reported resulting from an increase in the electric potential from 8 to 10 kV [28]. In another paper it was shown for electrospun PAN fibers that different applied voltages (10, 15 and 20 kV), did not cause significant changes in fiber diameter for solutions with various polymer concentrations [50]. Humidity tends to control the morphology of fibers including the surface topology [51–53]. Ref. [53] describes, for instance, the effect of humidity on fibers dealing with the development of porous fibers by elevated humidity during spinning. Temperature effects were found to influence the electrospinning process significantly, in particular as far as the average fiber diameter is concerned [51,54,55]. It was observed that increasing the solution temperature leads to a significant reduction in the mean fiber diameter. Yet such effects may also result from indirect effects originating from variations induced in parameters such as the evaporation rate of the solvent, the viscosity of the spinning solution.

These results on the impact of parameters on fiber formation part of which have already been summed up in previous review articles [1–7] were performed in general only on selected sets of polymers and of solvents considering in each case a restricted number of processing parameters. A disadvantage of such a restricted emperical approach obviously is that conclusions aiming at the control of the electrospinning process and the fiber production remain incomplete.

In order to account for the significance of multiple factors known to influence electrospinning, a theoretical analysis published in the literature has turned out to be very helpful [56]. It has allowed to find out how sensitive the electrospinning process and in particular the nanofiber diameter depend on the choice of spinning parameters and on the variations of the absolute values of these parameters. Considered was a set of 13 input parameters known from experimental investigations to affect the fiber diameters to various degrees. For these parameters starting values suggested by experimental results were selected which were subsequently subjected one by one to changes. Evaluated were the individually induced variations of the fiber diameters. The results were used to determine the significance of the individual parameters in controlling the evolution of the fiber diameter. The results show that five parameters (volumetric charge density, distance from nozzle to collector, initial jet/orifice radius, relaxation time, and viscosity) have the strongest effect on the jet radius. Predicted is a strong increase of the diameter with increasing volumetric charge density, initial jet/orifice radius, relaxation time and with decreasing nozzle distance and viscosity. Other parameters (initial polymer concentration, solution density, electric potential, perturbation frequency, and solvent vapor pressure) exhibit only moderate effects on the jet radius. A moderate diameter increase with increasing polymer concentration, decreasing solution density, increasing electric potential, increasing perturbation frequencies and increasing vapour pressure is predicted. Finally the parameters relative humidity, surface tension, and vapor diffusivity are predicted to display only minor effects on the jet radius.

So it is apparent that experimental studies as well as theoretical investigations have succeeded to a significant extent in unravelling the significance of major spinning parameters in controlling the fiber formation processes in electrospinning. Their effect on the stability of the spinning process, on fiber diameters, on fiber morphologies as well as topologies has been addressed. Nevertheless, there definitely is a need for further investigations addressing possible cross-talks between different processing parameters, modifications coming from changes in the spinning configurations but also aiming at pushing the level of understanding even more from a qualitative to a predominantly quantitative level.

2.3. Improvements and multiple extensions made to technical spinning devices

Starting from simple conventional syringe or single needle type electrospinning a broad range of improvements and extensions have been made more recently. These were aimed at enhancement of the stability of the spinning process, allowing to deposit the nanofibers in a highly control way along specific directions or even along predetermined pattern and aiming in particular also at enhancing the production rate considerably.

One such improvement comes from the gas-jet/electrospinning technique combining electrospinning with a gas-jet device [57–59]. In this technique the capillary through which the spinning fluid is pumped is surrounded circularly by a tube feeding a gas jet. The main difference between gas-jet/electrospinning and standard electrospinning is the additional drawing action of the gas jet imposed on the polymer fluid jet during the electrospinning process. The experimental results gained for instance for model systems of 25 wt% solutions of polyethersulfones (PES) in DMF showed that gas-jet/electrospinning causes the fibers to become more uniform and smaller in diameter while the production rate can also be increased. Choosing gas flow rates to be 5.0, 7.5, 10.0, 12.5, and 15.0 L/min as examples while keeping parameters such as the applied voltage, the inner diameter of the metal needle, the solution flow rate constant results were obtained showing that the average diameters of the PES fibers decreased monotonically as the gas flow rate increased. When the gas flow rate was increased from 5.0 to 7.5 L/min, for instance, the average diameter of the fibers decreased slightly from 424 to 393 nm. However, as the gas flow increased furthermore from 7.5 to 10.0 L/min, the average diameter of the fibers decreased remarkably from 393 to 208 nm. Finally as the gas flow was further increased, the average diameter of the fibers decreased only slightly from 208 to 183 nm. These results confirmed that the additional drawing action of the gas jet on the polymer fluid jet plays an important role during the electrospinning process.

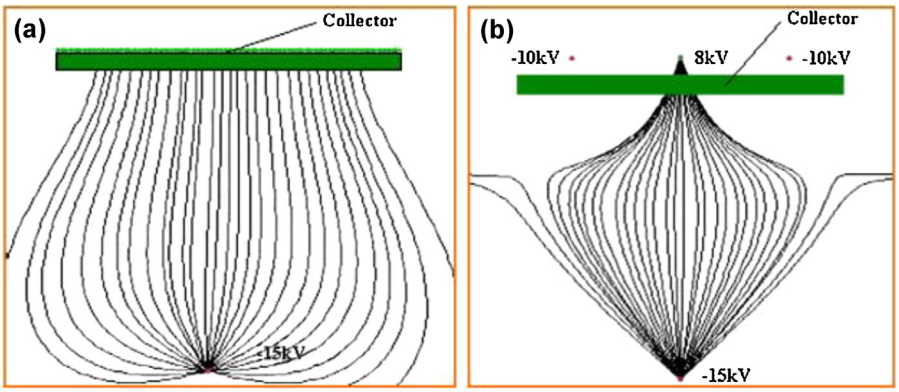

Fig. 2. Control of the electric fields in electrospinning via auxiliary electrodes placed on the backside—relative to the die electrode of a converging collector (a) homogeneous field, (b) converging field with the potentials applied to the auxiliary electrodes given. Reprinted with permission from ref. [60]. Copyrights (2007) Elsevier Ltd.

As far as the deposition of aligned fibers is concerned in electrospinning various approaches have been reported in the literature many of which were already described in previous review articles [1,3,4,7]. These include frame type counter electrodes, rotating cylinder or wheel type counter electrodes which will not be discussed here. One efficient method for controlling the width of electrospun fiber mats and for inducing fiber orientations in a micrometer and nanometer scale was achieved by stretching and converging the path of the fibers via the use of modified electrostatic field generated via an array of auxiliary electrodes [60–62]. These were placed, for instance, as apparent from Fig. 2 behind a rotating collector relative to the location of the die. Depending on the specific potentials applied to these electrodes homogeneous and converging fields were achieved [60].

The microstructure and alignment angles of these fibers relative to each other were characterized in these papers and compared with those of fibers produced without the use of auxiliary electrodes. The experimental results revealed that the percentage of micrometer fibers aligned relative to a specified direction increased from about 20% for electrospun mats prepared without any auxiliary electrodes, to more than 70% for mats produced using three auxiliary electrodes. When the distance between auxiliary electrodes was decreased, the resulting electrospun fibers became even more strongly oriented. The electrospun fibers at the boundary of the deposition area were observed to display about the same distribution pattern as those in the center of the electrospun mats. The alignment effect does not be changed when the diameter of the electrospun fibers is varied. These results are, of course, specific to the geometries of the setups used, but clearly display the potential for controlling fiber mat architectures through the use of auxiliary electrode arrays. It was further noted that the auxiliary electrodes had no profound effects on the average diameters of fibers.

Another approach towards fabricating well-aligned arrays and multilayer grids composed of nanofibers relies on a technique called magnetic electrospinning. In this approach, magnetic fibers are stretched into essentially parallel fibers over large areas (more than 5 cm × 5 cm) in a magnetic field [63,64]. Compared with other methods, magnetic electrospinning is reported to possess the advantages that the apparatus is simple and requires only adding two magnets to a conventional setup; that the magnetic field can be manipulated accurately; that the resultant nanofibrous arrays can be transferred onto any substrate with full retention of their structures; an advantage that can be further used to construct more complicated structures. Also the area of the aligned fibers is large compared to fibers generated with other methods. In magnetic electrospinning, the polymer solutions are typically functionalized by the addition of a small amount of magnetic nanoparticles. One model system evaluated was composed of poly (vinyl alcohol) (PVA) dissolved in distilled water at a concentration of 8 wt% into which Fe_3O_4 nanoparticles with an average diameter of 30 nm were dispersed [63]. The content of Fe_3O_4 in the electrospun fibers was found to be 0.22 wt %. When spinning the solution into fibers in the presence of a magnetic field generated by two parallel-positioned permanent magnets the magnetic field causes a stretching of the fibers across the gap of the magnet to form a parallel array. A conductive foil was placed between the bottoms of the magnets as an electrode. The length of the gap between the magnetic poles was varied in the investigations from several millimeters to several centimetres controlling thus the width of the resultant arrays.

Completely different approaches towards the deposition of nanofibers in a highly controlled way including the deposition following specific pattern rely on various types of modifications called near field electrospinning, high precision deposition electrospinning, direct writing by way of electrospinning all the way to electrodynamic jet printing [65–76]. Some of these were considered already in previous reviews [6,7]. Aiming at the integration of nanofibers into micro-fabricated microstructures such as structured electrodes tips shaped as arrows or triangles but also AFM tips acting as kinds of nozzles for electrospinning were used in several investigations [65–68]. These types of tips help in establishing Taylor cones for droplets attached to them. Droplets were formed at the tip either by dipping the tip into the spinning solution (model system PEO in a mixture of water and ethanol) [65] or by positioning the tip at the

exit of a microfluidic channel connected via a micropump to the reservoir of the spinning solution [66]. The tips were typically placed at a distance between 0.5 and 2 cm relative to the counter electrode connected to a translational stage and potentials of the order of 3–4 kV were used. Nanofibers were deposited, for instance, over etched trenches on a silicon wafer with fiber diameters – depending on the spinning solution, electrode distance, displacement velocities – between about 100 nm and up to about 1000 nm. In a similar approach called near field electrospinning a tip carrying a droplet is placed at a distance from about 500 μm up to 3 mm from the moving substrate and a minimum voltage of 600 V is used [67]. Here individual linear fibers in the diameter range between 50 and 500 nm were produced. Very recently atomic force microscopy (AFM) probe (nanometer size tip) has been utilized as an electrospinning tip for fabricating Nylon-6 nanofibers and depositing them in a controlled way within a 1 cm diameter area [68].

Syringe type electrospinning set-ups were also found to be able to deposit linear fibers along a predetermined direction [69–72]. In one approach syringes with an inner diameter of 100 μm, a collector distance of 500 μm and applied voltages of up to 1.5 kV were used. Large electric fields are required due to the small nozzle diameter to induce jetting [70]. This in turn was found to give rise to fibers with diameters in the range of a few micrometers. To reduce the fiber diameters by a reduction of the applied field below the critical one the recipe was to induce jetting via a tip used to draw mechanically single fibers from the charged droplet. Fiber diameters as small as 50 nm became accessible in this way using a voltage of 600 V and a 7 wt% PEO solution.

The so called High Precision Deposition Electrospinning (HPDE) [6,69,71] or direct writing approaches [72] rely on a conventional die-electrode/counter electrode set up with continuous pumping of the polymer solution through the die. The die/electrode to substrate/counter electrode distances are relatively reduced from the conventional ones (several cm to several 10 cm range) so that only the linear straight part of the jet path is formed and the bending instability is suppressed. The counter electrode and/or a planar substrate located on top of the counter electrode is mounted in this case on a displacement unit allowing shifts along the *X* and *Y* direction within the plane of the counter electrode as well as displacement causing a modification of the distance between the electrodes. The jet gives rise to the deposition of linear nanofibers along the substrate if the deposition speed and the displacement speed of the substrate are very similar typically in the range from about 10 cm/s up to several m/s depending on the die/substrate distance [71]. This enables the deposition of individual nanofibers or nonwovens in a highly controlled way both in terms of small fiber diameters and the location and orientation of the deposition. One is even able to "write" specific figures, pattern by moving the substrates along predetermined paths. For the case that the displacement speed is much smaller than the deposition speed the localized deposition pattern is found to display undulations along the fibers and even to become controlled by the onset of buckling processes giving rise to looping paths [71]. Also linear nonwoven paths with a path width in the range from 10 μm all the way up to cm can be produced in this way. Such writing has been achieved not only using spinning solutions but also polymer melts with typically higher viscosities and lower conductivities compared to polymer solutions [72]. Greater disturbance forces are required to overcome the surface tension in these jets, resulting in extended regions of stability up to many centimeters in length. Furthermore, these linear fibers can consistently be laid on top of each other to reproducibly build three-dimensional (3D) lattices. These were proposed for biomedical applications due to their dimensions that allow cell and tissue invasiveness.

Furthermore in a high efficiency electrospinning approach for deposition of ordered nanofibers an array of sharp tips was used to draw multiple polymer jets from the droplet to initiate electrospinning process under reduced voltage [73]. Also controlled continuous patterning of polymeric nanofibers on three-dimensional substrates using low-voltage near-field electrospinning in combination with a superelastic polymer ink formulation was reported [74] and finally a direct-writing technology based on near-field electrospinning was described which was used to fabricate an organic three-dimensional nanofibrous circle on the patterned silicon substrate [75].

One very effective approach for depositing nanostructures including linear structures and also complicated pattern is based not directly on electrospinning but rather on spraying [76]. Here a fluid flow is induced electrohydrodynamically through fine microcapillar nozzles used for jet printing of functional devices with submicrometer resolution. The droplet emerging from the nozzle is deformed and at a sufficiently high electric field droplets are ejected from the liquid cone in a controlled spraying mode. The printing of complex patterns with ink composed of conductive or insulating polymers but also of nanoparticles, nanorods, nanotubes is illustrated in the paper. Furthermore an electrohydrodynamic printing method that can be used to create ordered structures and complex pattern using coarse processing needles is reported [77].

Coming to the topic of enhancement of the production rate of electrospinning it is well known that many nanofiber applications such as filter, textile and even tissue engineering applications need large quantities of fibers. Electrospinning relying on a single syringe type spinning tends to produce nanofibers at a very slow rate of around 0.01–0.1 g/h. A straightforward method towards production enhancement is based on increasing the number of needle nozzles [4–7]. However, the multi-needle set-up needs a large operating space and careful design of the relative spacing between the needles so that strong charge-repulsion between the jets and adjacent needles can be minimized and the associated uneven fiber deposition can be avoided. In addition, clogging of the needles contributes to discontinuity of the electrospinning process.

The formation of multiple jets was reported for the case of porous tubes – pores with an average pore size typically in the range of 20–40 μm – with walls of uniform thickness and uniform flow resistance [78,79]. The polymer solution passes through the wall to emerge at points randomly distributed over the whole surface of the tube [78]. In a modified approach small holes were drilled half way through the porous wall [79]. The purpose was to create points of

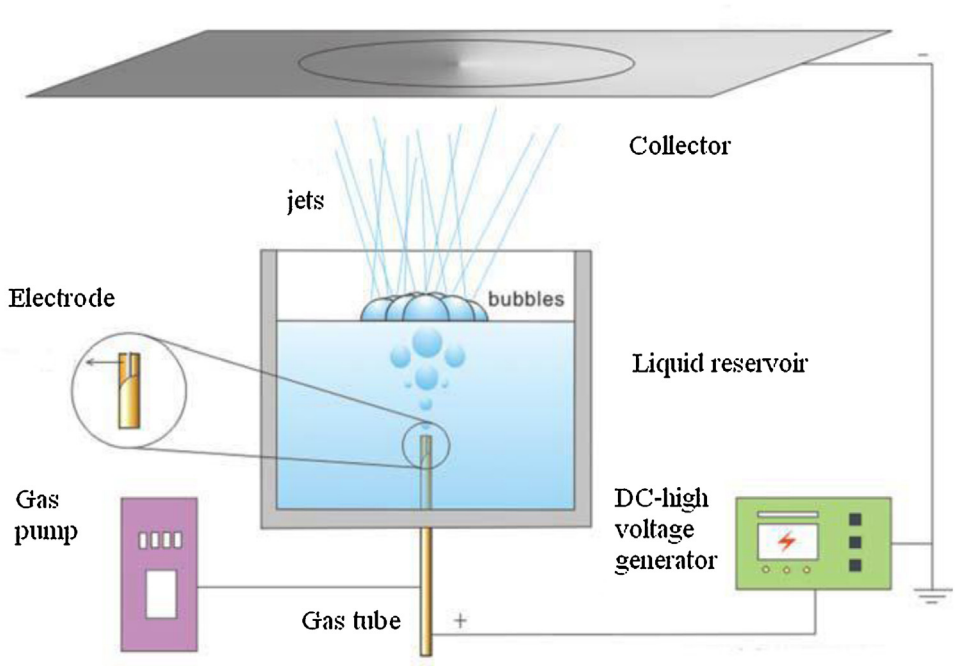

Fig. 3. Sketch of the set-up used in bubble electrospinning. Reprinted with permission from ref. [82]. Copyrights (2010) Wiley Periodicals, Inc.

lesser resistance through which the polymer solution preferentially flows at predetermined locations. The polymer solution inside the tube has to be pressurized sufficiently – air pressure of the order of up to several kPa – to force the polymer to flow through the drilled holes but not elsewhere. A wire electrode is located in this approach inside the tube to maintain an equal electrical potential in the tube even in poorly conducting liquids. Each hole was found to produce one jet for which at a distance of a few centimetres from the origin the electrical bending instability becomes dominant and the jet forms an expanding coil with the electrical repulsion between the adjacent jets maintaining their separation. The device was reported to produce fiber mats at mass rates greater than known from a single electrospinning with fiber diameters in the several 100 nm range. The narrowest size distribution and smallest fibers were experienced, for instance, for potentials of about 50 kV. In all cases the average fiber diameters achieved were between 0.3 and 0.6 μm. To determine the mass production rate the mass of fiber collected on the aluminum foil during a 10 min interval was measured. The result shows that this method can produce fiber in the range of 0.3–0.5 g/h for a 13 cm long tube with 20 holes on the bottom surface of the tube. Electrospinning production rates from a single nozzle (needle or pipette) are typically 0.01–0.1 g/h as discussed above. This shows that the production rate from the porous tube is about 5 up to 30 times higher.

A set of further designs were developed relying on the socalled needleless spinning. In neeedleless spinning the electric field is no longer concentrated on the tip of the needle but it is concentrated in a large area. Pioneering work was reported by Yarin and Zussman [80] who used a magnetic fluid to agitate the uppermost polymer solution to thus initiate multiple jets from a flat polymer solution surface. Protrusion were created on fluid surfaces by inducing statistical surface roughness modulations via superparamagnetic particles immersed in the spinning solution via their interactions with magnetic fields. Magnetic fields tend to induce spike structures for such systems as known from magnetic fluids. Other approaches reported in the literature include rotating charged electrodes for which part of their circumference are immersed in polymer solution to pick up polymer solution onto the electrode and the use of a rotating cone to generate needleless electrospinning with high production rate as described in review papers [7].

In bubble electrospinning processes compressed gas is released inside the solution producing one or several bubbles on the free surface of the solution as shown in Fig. 3 [81–84]. The bubble stretched upward on exposure to an electric field and deformed to an oval shape and finally to a conical shape with the whole process taking about 17 ms. From the conical bubble, a jet is ejected, and then the bubble is observed to burst and further to split into numerous jets. Finally almost the whole liquid film is broken into thin jets. Then, the next bubble is produced, and the process is repeated until the polymer solution is used up. This technology was demonstrated to be able to produce nanofibers as small as 50 nm and the fiber diameter is found to increase with increasing voltage. Using PVP fibers spun from 36 wt% solutions of PVP in a mixture of pure alcohol/distilled water (9:1, w/w) as example, the average diameter of fibers could be increased from 860 to 1180 nm, with the increase in the applied voltage from 16 to 35 kV.

The effect of the polymer concentration in the spinning solution was also investigated. For low concentrations fibers cannot be spun, beads appear as the concentration is close to the threshold value for fiber spinning,

this phenomenon is similar to that in classic electrospinning. Fibers with larger diameter and smooth surfaces are obtained for larger concentration. As far as the production rate of fibers produced by bubble electrospinning is concerned it turned out to be in the range of 7.5 g/h using a single bubble electrospinning approach. The production rate is much higher than the one in traditional electrospinning even if spinning is restricted to single bubbles. Yet it has been found that one may succeed in producing several or even scores of bubbles on the surface of polymer solution causing a further strong increased output. Adjusting the gas pressure the number of bubbles produced on the surface of a PEO model solution amounted typically at appropriate conditions to 1, 5, 14, 17 and more bubbles.

Furthermore a conical wire coil was successfully used to generate needleless electrospinning of nanofibers [85,86]. An advantage is that it can concentrate much higher electric fields on the surface of the coil and can thus produce not only fibers in a larger quantity but also finer nanofibers than needle based electrospinning systems. Multiple polymer jets were produced on the surface of the coil during the spinning process. The productivity of this needleless electrospinning was 20–60 higher than that of needle electrospinning, and the productivity was greatly increased by increase of applied voltages and decrease of collecting distances for given polymer concentrations. For a given applied voltage and collecting distance, the productivity decreased for a model PVA spinning solution with the increase of the PVA concentration due to its higher viscosity. The fiber diameter and diameter distribution was furthermore found to be greatly influenced by experimental parameters such as the PVA concentration, applied voltage, and collecting distance. This novel concept of using a conical wire coil nozzle has obviously the potential to contribute to further developments of large-scale needleless electrospinning system for nanofiber production.

The range of nanofiber architectures accessible by electrospinning has become strongly extended by the introduction of coaxial electrospinning in 2003 [80]. Although being developed rather recently coaxial electrospinning has already experienced strong progress in terms of fiber structures achieved, modifications to which it has been subjected and in terms of modelling and subsequent experimental and theoretical developments reported in the literature as obvious from corresponding reviews [88,89]. In coaxial electrospinning, in principle, an inner and an outer die arranged in a concentric geometry allowing to pump two different spinning solutions simultaneously is used to produce a core shell droplet at the exit [87]. In close analogy to conventional electrospinning the droplet becomes deformed in the presence of an applied electric field and at sufficiently strong electric fields a compound jet emerges from the tip of the deformed droplet. This compound jet experiences the well known bending instability further down along its path inducing strong jet stretching and jet thinning. Finally a thin solid core shell fiber is deposited on a substrate. The range of materials selected for the preparation of the core has, as obvious from the literature, become extremely broad [89] and includes polymers, nonpolymeric Newtonian fluids – such as water, oil – as well as nanoparticles, nanoscalar biological objects with the shell material tending to be of polymeric nature including natural and synthetic polymers.

The modelling of the formation of core shell jets and of the complex structure formation processes controlling the final structure of the core shell fibers has been the topic of set of papers [96–98]. Simulations have revealed that the electric charges concentrate at the outer surface of the compound jet in the presence of an applied field so that the uncharged core droplet can become incorporated into the shell jet only by viscous forces. Further theoretical analysis has revealed that the core shell jet tends to be subjected to a set of instabilities controlling a complex structure formation in the resulting nanofibers including the break up of the core into separate droplets located inside an intact shell. Furthermore jet buckling of the nanofibers originating from longitudinal compressive forces may take place if the core and shell solutions are fed with different rates.

Coaxial electrospinning can be used not only for the preparation of core shell fibers but also of nanotubes by various approaches. In a one-step approach core shell jets are produced based on two different polymers dissolved in two different solvents [92]. Detailed studies have identified conditions for tube formation in this approach. These include a fast solidification of the shell solution and an enhanced wetting of the shell by the core solution. Hollow structures also arise if the core is removed after the deposition of solid core shell fibers via coaxial electrospinning. This approach has been employed to prepare among others hollow polymer nanotubes, carbon nanotubes [88] but also ceramic ones [93,94]. Coaxial spinning of a mixture of PVP with a titanium precursor as shell and mineral oil as core may serve as an example. Here the mineral oil was subsequently removed to yield a hollow fiber. After a thermal removal of PVP and the calcination of the precursor titania nanotubes resulted. Carbon nanotubes become accessible via core shell fibers from poly(methyl methacrylate) (PMMA) as core and PAN as shell by subjecting the fibers to a two step heating process involving the decomposition of the PMMA and the carbonization of PAN at much higher temperatures [91].

It has furthermore been demonstrated that electrospinning of core–shell polymer nanofibers can also be achieved via single-nozzle electrospinning setups using emulsions of two polymer solutions as shown schematically in Fig. 4 [95]. Solutions of PMMA in DMF and PAN in DMF which decompose in blends into PMMA/DMF droplets dispersed in the PAN/DMF matrix have served as example. In principle, the as-spun fibers should not possess an intact PMMA core yet the number of core disruptions was found to be very small. The reason for this is the very strong stretching of material elements in the co-electrospun jet. Co-electrospinning of core–shell nano- and microfibers from a single nozzle were also reported in several other papers [96–99].

Potential applications of co-electrospinning evaluated in the literature include the encapsulation of non-spinnable polymers, of non-polymeric materials in the core of the nanofiber as detailed in review papers [88,89]. Numerous

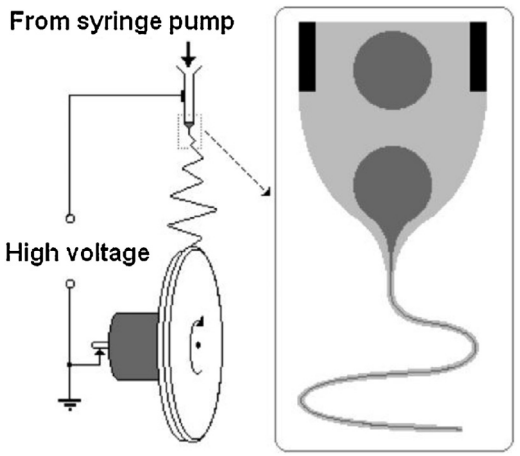

Fig. 4. Single nozzle electrospinning of polymer emulsions yielding core shell fibers. Reprinted with permission from ref. [95]. Copyright (2007) American Chemical Society.

papers have dealt with applying co-electrospinning for the encapsulation of drugs or biologically active objects in the fiber core. It has been found out that the release rate from nanofibers is controlled in general by the desorption of the incorporated functional molecules from the surfaces directly exposed to the surrounding fluid environment rather than by solid-state diffusion as was assumed before [100]. To allow release of functional molecules located in the core surrounded by a perfectly intact shell, materials which rapidly dissolve in water, leaving open pores, have been added in the shell. It is important to point out that biologically active objects are protected not only from the solvents in the shell solution but also from the effect of the electric charges [90]. A broad range of investigations has also addressed nanofluidic applications considering pressure driven-flows inside co-electrospun fibers [88,89,101,102] as well as the production of therapeutically valuable nanoparticles [103].

Finally it should be pointed out that coaxial electrospinning can apparently not only be used to produce core shell and hollow nanofibers but rather also to improve the quality of monolithic nanofibers [104–106]. To demonstrate this, a polymer solution was fed to the core die whereas salt solutions or appropriately selected solvent mixtures were used as shell fluids. Exploiting this approach fibers with smaller diameters, smoother surfaces and with more uniform structures are reported to become accessible.

To conclude, the technical progress that has been made more recently in designing novel spinning configurations, modes of fiber depositions, preparation of complex fiber architectures is impressive. Based on this progress the assembly of fiber-based nano- and micro devices relying on electrospinning has approached reality. Ongoing investigations have the enhancement of the production rate as one key goal and a lot of surprises can be expected in this area.

3. Materials: functions and technical application aspects

3.1. Nanofibers composed of metals, metal oxides, ceramics and composites with organic polymers

An area in electrospinning which has developed strongly in the last few years is the preparation of nanofibers composed purely of metals, of metal oxides, and sulfates respectively, ceramics or composites of such materials with organic polymers. These types of nanofibers exhibit in general specific electronic, photonic and magnetic properties. Examples in case are nanofibers displaying properties such as fluorescence, electroluminescence, enhanced ion or electron conductivities, photovoltaic effects, photocatalytic effects, ferromagnetism, superparamagnetism. Applications of such nanofibers investigated in the literature and reviewed below include optical and electronic sensors, lithium ion batteries, fuel cells, solar cells, as well as energy harvesting and storage systems. Main reasons for choosing nanofibers as elements for such applications are the one-dimensional nature of the nanofibers affecting opto-electronic properties, the large specific surface coming with the nanoscale, short electronic diffusion distances across the fiber diameter and the high porosity of the nonwovens of up to 90% obtained via electrospinning.

Electrospinning has been exploited for the preparation of metal, metal oxide, semiconductor nanofibers, and of the corresponding polymer composites either by combining it with sol–gel processes or by following a polymer-based precursor route. Precursors of the target materials such as metal salts are introduced for this purpose into spinning solutions containing polymers and an appropriate solvent able to solve both the polymer and the salts as reported in previous reviews [4,6]. Electrospinning of such a ternary solution is found to give rise to polymer nanofibers in which the salts are homogeneously dispersed provided that the spinning parameters are chosen appropriately. The precursor materials are, in a subsequent step, reduced to the target metals or metal oxides via thermal treatment or the treatment in the presence of reducing agents such as, for instance, hydrogen. The results are polymer composite nanofibers. In a further step the polymer can be removed completely, in general again by thermal treatment to yield nanofibers from the pure metal, metal oxide materials, for instance. Here previous reviews published in the last few years highlight material aspects [4,6,7] so that the present report will focus predominantly on electrospun fibers exhibiting specific electronic, photonic and magnetic properties stressing both the aspect of functions and of selected applications.

3.2. Electrospun fibers exhibiting specific photonic and magnetic functions

3.2.1. Luminescent nanofibers

One dimensional (1D) nanostructures displaying luminescence i.e. photoluminescence, electroluminescence have attracted strong attention in recent years in particular in view of potential applications in light emitting diodes, full colour displays, lasers, data storage [107]. The

number of papers on electrospun light emitting nanofibers has correspondingly increased strongly with the last years. In principle three concepts were used to prepare such nanofibers based on (a) conjugated polymers frequently in combination with polymer blend components, (b) polymers into which functional components such as quantum dots or rare earth complexes were incorporated (here the argument is that such an approach allows to combine the favorable properties of the organic materials – flexibility, processibility, light weight – with the ones of the inorganic materials – hardness, thermal stability, chemical resistance, optical function), (c) inorganic materials doped among others also with rare earth complexes.

3.2.2. Conjugated polymer-based nanofibers

Luminescent polymer nanofibers with diameters in the range from 250 to about 750 nm were obtained from binary blends of a set of conjugated polyfluorene (PFO) derivatives with PMMA [108]. Homogeneously mixed nanofibers were observed for lower concentrations of the PFOs while core shell fibers were found for higher PFO concentrations. Phase separation caused by the lower solubility of PFOs in the common solvent was proposed to be the origin of the core shell formation. Strong blue, green, yellow and red luminescence was observed depending on the type of PFO derivative. One conclusion was that the polyfluorene aggregates are much smaller in the fibers compared to a spincoated film causing a blue shift of the emission and a higher luminescence efficiency. Blends were also considered for the conjugated polymer poly (2-methoxy-5-(2′-ethylhexyloxy)-1,4-phenylene-vinylene) (MEH-PPV) with PVP [109,110]. Both homogeneous fibers obtained from a single die set-up and core shell fibers obtained via coaxial electrospinning with MEH-PPV being the shell were investigated. In addition pure MEH-PPV fibers were prepared by removing the PVP from the homogeneous fibers. Reported was the display of fluorescence in all cases with the fluorescence being outstanding for the core shell system. Furthermore nanofibers composed just of MEH-PPV and of the conjugated polymer poly (3-hexylthiophene) (P3HT) were prepared [111]. They were deposited in a highly aligned way allowing thus investigations on the optical anisotropy of the fibers induced by electrospinning. In fact, it was found that the emission was much stronger along the nanofiber axis as compared to the perpendicular direction. Similar findings were reported for other types of conjugated polymers [112]. Here polarized IR spectroscopic investigations and micro-Raman investigations showed strong orientational order within the nanofibers. Electroluminescence in addition to fluorescence was detected for nanofibers composed of blends of the conjugated polymer poly [(9,9-dioctylfluorenyl-2,7-diyl)-alt-co-(1,4-benzo-{2,1′,3}-thiadiazole)] (F8BT) in polystyrene (PS) or poly(ethylene oxide) (PEO) [113]. Ribbonlike nanofibers composed of the electroluminescent polymer (F8BT) were used as active material in a planar organic light emission diode type architecture (OLED) as depicted in Fig. 5. Here electrical connection was achieved by incorporating F8BT fibers of about 700 nm width and 110 nm height into a single layer device the architecture of which tends to induce charge recombination on the conjugated polymer nanofiber. The

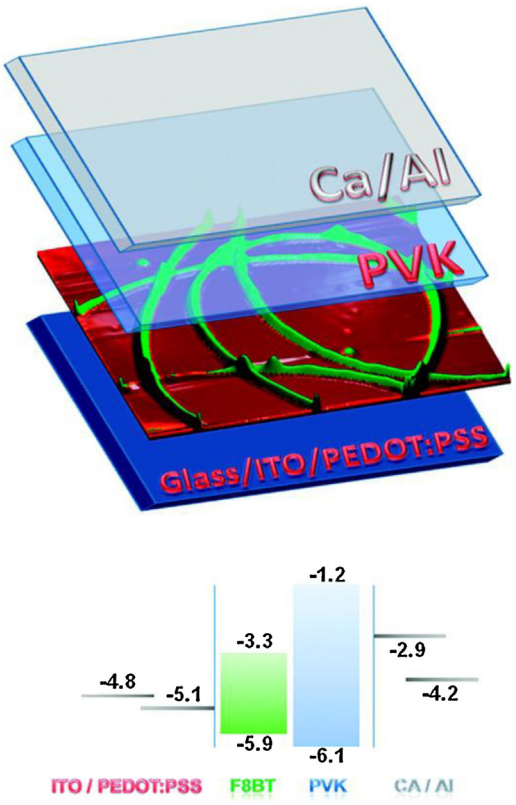

Fig. 5. Planar organic light emission diode type architecture (OLED) with ribbonlike nanofibers of an electroluminescent polymer (F8BT) as active material, PEDOT/PSS: Poly(3,4-ethylenedioxythiophene) poly(styrenesulfonate), PVK: poly(*N*-vinyl carbazole). Reprinted with permission from ref. [113]. Copyright (2011) American Chemical Society.

diode was characterized by a brightness of 2300 cd/m^2 at 6 V.

3.2.3. Polymers nanofibers doped with luminescent components

Components used to induce luminescence in polymer nanofibers include quantum dots as well as rare earth complexes, in particular europium and erbium complexes. Nanofibers prepared from poly(ethylene oxide) containing ZnO quantum dots showed a significant quenching of the visible emission of the quantum dots [114]. The quenching was attributed to the formation of O–Zn bonds at the surface of the quantum dots. In other studies fibers composed of CdSe/ZnS quantum dots incorporated into cellulose triacetate showed a substantial fluorescence already at small concentrations of the quantum dots [115]. Birefringence investigations revealed again a considerable alignment of the polymer chains along the nanofiber axis. To prepare CdS nanocrystals inside electrospun polymer fibers an approach based on the decomposition of cadmium thiolate precursor was proposed [116]. Strongly light emitting fibers are reported for such composites. PPV/PVA composite nanofibers into which Ag_2S nanocrystals were introduced were achieved by spinning a solution containing in addition to PVA a sulfonium precursor of PPV and silver nitrate followed by a conversion step [117]. Such

nanofibers were reported to display a significant photoluminescence. To prepare nanofibers composed of PPV as conjugated polymer and TiO_2 nanoparticles, the nanoparticles were introduced into the solution with the PPV precursor [118]. After a thermal conversion of the fibers composed of the PPV precursor, composite fibers were obtained showing outstanding emission properties.

A set of polymers including PVP [119,120], PS, PMMA [119] and polyimide (PI) [121] were doped with Europium complexes. It is well known that such complexes have good luminescent properties because of the antenna effect of ligands and the f–f electron transition of the Eu^{3+} ions. The luminescent properties were studied in the composite nanofibers in comparison to those of the pure complexes. The results show strong emission in all cases with the observation being that in all of the composite fibers the excitation bands of the ligands split into different components due to decreased symmetry in the composites. In addition, the thermal stability of the photoluminescence of Eu^{3+} in the composite fibers is considerably improved over that of the pure complexes. Furthermore photoluminescence properties were studied for PVP nanofibers doped with Re(I) complexes [122]. A bright yellow emission peaking at 543 nm is observed for these composite fibers, and this emission is attributed to the triplet emissive state of the Re(I) complex.

3.2.4. Inorganic luminescent nanofibers

A significant number of investigations have considered inorganic electrospun fibers doped with rare earth complexes such as ones based on Erbium (Er), Europium (Eu), Terbium (Tb), Samarium (Sm), Cerium (Ce), Dysprosium (Dy) [123–136]. The rare earth metals lanthanoides form a group of chemically similar elements which have an open 4f shell in common. Lanthanoides absorb radiation in very sharply defined bands (4f–4f transition). The f–f transitions of free lanthanoid ions are forbidden. When the centrosymmetric symmetry of the ion is removed by an asymmetrical external crystal field, the transitions become allowed: the luminescence of complexed lanthanoides is enhanced. The number of luminescent nanofibers electrospun from inorganic materials containing Europium complexes is considerable. The general observation is that these complexes control the emission properties to a major extent with modifications coming from the nanofiber matrix. The range of inorganic materials used for Europium doped nanofibers include titania nanofibers [123,124], oxynitride phosphor materials consisting of $CaSi_2O_2N_2$ [125], ZnO nanocrystals uniformly dispersed in nanofibers (reported is an efficient energy transfer for enhanced red emission from Eu^{3+} in polymer nanofibers composed of Eu^{3+} doped ZnO nanocrystals) [126], YBO_3 and $GdBO_3$ nanofibers (the annealing temperature is reported to have strong effects on the crystallization and luminescence properties). Photoluminescence spectra indicate that higher temperatures result in improved fluorescence capability.

A further set of inorganic luminescent nanofibers were based on doping with Tb complexes. These include as fiber material $CaWO_4$ (blue emission) [127], β-Ga_2O_3 (under UV excitation, the β-Ga_2O_3:Tb^{3+} samples showed green emission with the strongest peak at 550 nm) [128], Gd_2O_3 (the obtained Gadolinium nanofibers have an average diameter of about 80 nm and are composed of pure cubic Gd_2O_3 phase) [129], titania [130], Y_2O_3 (Yttrium oxide nanofibers) [131] and La_2O_3 (lanthanum oxide) [132]. Furthermore fibers composed of $Ca_4Y_6(SiO_4)6O$ were doped with Tb complexes [133]. In addition fibers from $GdVO_4$ were doped with Dy and Sm complexes [134] and titania nanofibers with Lanthanium (La) and Erbium (Er) complexes [124,135,136]. The erbium doped titania nanofibers were reported to be strongly emissive in the near-infrared at 1540 nm with the intensity being directly proportional to erbium concentration. Y_2O_3 (Yttrium oxide) nanofibers were doped with rare earth ions Sm and Dy [131], titania nanofibers were doped with ytterbium [130], $SrAl_2O_4$ fibers with Ce [137], titania nanofibers with La and erbium complexes [124,135,136]. The erbium doped titania nanofibers were found to be strongly emissive in the near-infrared at 1540 nm. The intensity is reported to be directly proportional to erbium concentration.

Other types of luminescent electrospun fibers of inorganic nature reported in the literature are anatase TiO_2 nanofibers (the sintered fibers were polycrystalline. and composed of densely packed TiO_2 grains with the size amounting to 12 nm) [138], Carbon/CdS coaxial nanofibers (the fibers displayed both photoluminescence and conductive properties, the photoluminescence originating from the CdS quantum dots) [139], BCNO phosphor (the nanofibers showing intense green and yellow emissions under UV-light irradiation that could be seen by the naked eye) [140], ZnO (showing in photoluminescence a near-UV peak corresponding to near-band-edge emission and a strong broad peak in the visible regime) [141], and Cd/CdO (here for the first time pure Cd metal could be successfully incorporated in a 1-dimensional nanostructure) [142].

So, a broad range of one dimensional – i.e. fiber type – nanostructures exist today which display specific photonic properties of interest for various types of applications including light emitting diodes or even lasers. These fibers are based on both pure organic materials and doped organic as well as inorganic materials. Particularly promising seem to be systems doped with rare earth complexes. What is missing to a certain extent at this stage is the development of device architectures taking full advantage of the specific properties of the phonotic electrospun fibers.

3.2.5. Nanofibers with specific magnetic properties

1D magnetic nanomaterials are meeting with significant interest in view of the unique phenomena observed for the case that the geometrical dimensions of the material become comparable to critical sizes specific for each ferromagnetic material (examples: Fe: 14 nm; Ni: 55 nm; Fe_2O_3: 128 nm). Single domain nanoparticles without domain walls are known to be stable at such sizes with the spins being strongly affected by thermal fluctuations. Isolated nanoparticles display superparamagnetism characterized by the absence of a permanent magnetization and a "hysteresis" with the coercivity being zero. Fibers composed of isolated nanoparticles tend thus to display superparamagnetism while fibers composed of particles with aspect ratios larger than 1 all the way up to single domain

rods tend to exhibit ferromagnetism while intermediate states – simultaneous display of superparamagnetism and ferromagnetism – can also occur. Magnetic nanowires have become targets for utilization in high-density magnetic recording, spintronic devices, magnetic sensors and magnetic composites. Magnetic nanowires are also scientifically interesting because they act as model systems for the study of interaction processes and magnetic reversal in low-dimensional magnetic structures.

A wide variety of nanofibers with specific magnetic properties were prepared via electrospinning based on polymer composite fibers with dispersed magnetic nanoparticles, based on metals such as cobalt, iron, nickel, on metal oxides or also based on composite materials with highly complex compositions as known from bulk magnetic materials. An interesting case is reported for poly(vinylidene difluoride) fibers containing various concentrations of ferrite ($Ni0.5Zn0.5Fe_2O_4$) magnetic nanoparticles [143]. The amount of the ferroelectric β and γ phases present in the fibers was found to increase with increased nanoparticle loading. Magnetic PAN-Fe@FeO nanocomposite fibers were prepared by different core–shell Fe@FeO nanoparticles loadings [144]. Electrospun PVP fibers were prepared containing different proportions of ferromagnetic and superparamagnetic nanoparticles [145]. Very high magnetic nanoparticle loadings of up to 50% were reported and a very high magnetization (amounting to about 25 emu/g) was observed. Also a mixed superparamagnetic/ferromagnetic behavior was demonstrated. Nanocomposites displaying a giant superparamagnetic response were synthesized by employing natural horse spleen ferritins embedded in PVA nanofibers [146]. The transmission-electron-microscopy images of these samples showed different distributions of ferritins in the PVA nanofiber affecting the superparamagnetic properties.

Cobalt and iron nanofibers produced by a polymer precursor route revealed ferromagnetism with the hysteresis loops being strongly different for the cases that the magnetic fields were oriented parallel and perpendicular respectively relative to the fiber axes [147]. Along the same line oriented fibers composed of nickel, cobalt and iron with diameters down to about 25 nm were produced displaying enhanced coercivities relative to the corresponding bulk materials [148]. Such enhanced coercivities were also reported in another publication on nickel nanofibers [149]. Magnetic Fe_2O_3 hollow fibers were obtained based on PVP as precursor polymer [150]. At room temperature the hysteresis properties are found to be strongly controlled by the size of the nanofibers. The coercivity force increases with the average diameter while the remnant magnetization decreases. Magnetic moment vs. temperature diagrams for samples with different average diameters (Fig. 6) show two magnetic transitions assigned to Morin transitions (The Morin transition T_M is a magnetic phase transition in α-Fe_2O_3 hematite where the antiferromagnetic ordering is reorganized from being aligned perpendicular to the *c*-axis to be aligned parallel to the *c*-axis below T_M).

Magnetic cobalt ferrite ($CoFe_2O_3$) nanofibers, nanoribbons, nanotubes but also copper ferrite nanofibers ($CuFe_2O_3$) were produced by electrospinning with PVP as precursor polymer displaying fiber diameters down to about 70 nm and up to several 100 nm [151]. Furthermore nickel–iron/nickel ferrite composite nanofibers were reported exhibiting strongly enhanced coercitivities and saturation magnetizations as compared to pristine nickel ferrite nanofibers.

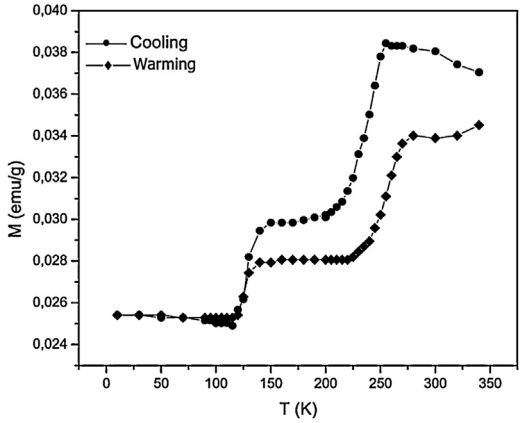

Fig. 6. Magnetic moment versus temperature behavior for magnetic Fe_2O_3 hollow fibers with an average diameter of 200 nm observed for cooling and subsequent heating runs at an applied magnetic field of 25 Oe. Reprinted with permission from ref. [150]. Copyright (2011) American Chemical Society.

A simple procedure has been described in the literature for the preparation of magnetic high aspect ratio nanotubes composed of α-Fe_2O_3 and Co_3O_4 with diameters less than 100 nm and wall thicknesses less than 25 nm based on an appropriate heat treatment of electrospun polymeric fibers containing Fe(III) and Co(II) ions [152]. Electrospun $BiFeO_3$ nanofibers were reported to display multiferroic properties. Multiferroics are defined as materials that exhibit more than one primary ferroic order parameter – primary ferroic order parameters being ferromagnetism, ferroelectridity and ferroelasticity – simultaneously [153]. Multiferroic $CoFe_2O_4$-$Pb(Zr_{0.52}Ti_{0.48})O_3$ core–shell nanofibers were furthermore synthesized by coaxial electrospinning in combination with a sol–gel process [154]. The multiferroic properties of core–shell nanofibers were demonstrated by magnetic hysteresis investigations and via piezoresponse force microscopy. For nanofibers composed of $Co_{1-x}Zn_xFe_2O_4$ $(0.0 \le x \le 0.5)$ ferrites with diameters of 110–130 nm variations of the coercivity and the saturation magnetization with the calcination temperature were found obviously originating from grain-size effect [155]. Magnetic diphase nanofibers composed of $ZnFe_2O_4$/γ-Fe_2O_3 were synthesized by electrospinning a sol–gel solution containing a molar ratio (Fe/Zn) of 3 [156]. The effects of the calcination temperature on the phase composition, particle size and magnetic properties were investigated. For yttrium iron garnet (YIG) $Y_3Fe_5O_{12}$ nanofibers room temperature ferromagnetism with a well formed M–H hysteresis loop and with about 70% of the remnant magnetization relative to the saturation value was reported [157]. The range of composite materials used to prepare magnetic fibers is, in fact, very impressive. Nanofibers electrospun from such composites include $SrFe_{12}O_{19}/Ni_{0.5}Zn_{0.5}Fe_2O_4$ composite ferrite nanofibers [158], ferromagnetic $Y_3Fe_5O_{12}$ nanofibers

[157], $Sr_{0.8}La_{0.2}Zn_{0.2}Fe_{11.8}O_{19}$ nanofibers [159], composite $Ni_{0.5}Zn_{0.5}Fe_2O_4/Pb(Zr_{0.52}Ti_{0.48})O_3$ nanofibers [160], $Sr_{1-x}La_xZ_xFe_{12-x}O_{19}$ nanofibers where the effect of La–Zn substitutions on microstructure and magnetic properties were investigated [161], $La_{0.67}Sr_{0.33}MnO_3$ nanowires with large low field magnetoresistance [162], $Ba_{(1-x)}La_xFe_{12}O_{19}$ nanofibers, where magnetic and microwave absorbing properties were investigated [163] and diluted magnetic semiconducting Co-doped zinc oxide ($Zn_{1-x}Co_xO$) (x = 0, 1.8, 4.4, and 7.2 at.%) nanogranular nanofibers with diameters of 70–250 nm for which exciton quenching and a ferromagnetism-to-ferrimagnetism crossover was reported [164].

It has become apparent that nanofibers have been successfully prepared via electrospinning showing a broad range of magnetic properties including ferromagnetism, superparamagnetism, multiferroic properties as well as Morin transitions. One of the interesting findings is that the grain size within the fibers can be used to tune properties such as the coercivity or the saturation magnetization. Quite impressive is furthermore the strongly controlled design of magnetic fibers with highly complex compositions. Future studies will certainly consider applications of magnetic fibers such as magnetic sensors, flexible magnets, biosensors, anti-counterfeiting elements.

3.3. Electrospun nanofibers as key elements in optoelectronic devices

3.3.1. Sensors

Nanofibers fabricated via electrospinning have specific surfaces approximately one to two orders of the magnitude larger than flat films, which makes them excellent candidates for potential applications in sensors. Nanofiber-based sensors are targeted, for this reason, to show much higher sensitivity and quicker responses compared to sensors based on flat films. Nanofiber designs have very frequently been developed to act as sensitive, fast, stable and reproducible gas sensors which can easily be integrated into a multi-component array [165]. A gas sensor is a device which detects the presence of different gases in a given area for monitoring environmental pollution focusing frequently on those gases which might be harmful to humans or animals. Sensor performance features such as sensitivity, selectivity, time response, stability, durability, reproducibility, and reversibility are known to be largely influenced by the properties of the sensing materials used. It is for this reason that a broad range of materials such as semiconductors (semiconducting metal oxides such as TiO_2, SnO_2, ZnO), organic/inorganic composites, conducting polymers, carbon graphites have been investigated for sensing devices based on electrospun fibers.

3.3.2. Polymer composite sensors

Polymer microfibers encapsulating polydiacetylene (PDA) chain molecules known to be active as chemosensors and photonic materials were prepared via electrospinning and subsequent UV irradiation of self-assembled diacetylene monomers in the fibers yielding blue-colored PDA-containing polymer fibers [166]. The feasibility of using PDA-embedded electrospun microfibers as potential sensor materials was demonstrated by fluorescence generation as controlled by specific ligand–receptor interactions. A composite comprising poly(vinylidene fluoride) (PVDF) and poly(aminophenylboronic acid) is reported to display an excellent linear response to the detection of glucose for the concentration range from 1 to 15 mM with a response time of less than 6 s [167]. Composite nanofibers of conducting polymers and hydrophobic insulating polymers, composed of polymers based on pyrrole and PS or PMMA respectively, were prepared and the sensing properties were studied relative to chloroform and ammonia [168]. PAN/zinc chloride ($ZnCl_2$) composite nanofibers were observed to display an enhanced sensing response to hydrogen sulfide [169]. Porphyrin/PVA nanofibers were found to show a significant acid vapor sensing capability [170]. Gold nanoparticles were prepared via in situ synthesis on porous PAN nanofibers to form an electrochemiluminescent (ECL) sensor [171]. Resistive relative humidity (RH) sensors were fabricated by nano composites of nylon-6 and titanium dioxide nanopowders. The results indicated that these sensors can be fabricated as reliable, low cost and fast response devices [172]. A single PANI nanofiber field effect transistor (FET) gas sensor was fabricated with the nanofiber transistor showing a 7% reversible resistance change to 1 ppm NH_3 with a gate voltage of 10 V [173]. PANI/titanium dioxide (PANI/TiO_2) composite nanofibers were prepared by combining the electrospinning technique with chemical oxidation. They display good sensing property for ammonia gas [174]. Polyvinylpyrrolidone (PVP)/multiwall carbon nanotubes based Surface Acoustic Wave (SAW) sensors were fabricated and their sensitivity towards hydrogen gas investigated [175]. Reported is also the use of electrospun nanofibrous film for surface acoustic wave (SAW) sensors to enhance their chemical detection capability. Ultrafine (100–300 nm) poly(ethylene oxide) (PEO) fibers with controlled thickness and porosity were electrospun for this purpose and coated on the surface of a quartz SAW sensor [176]. A phosphorescent Cu(I) complex has been incorporated into a PS matrix and the use of the composite microfibrous membranes as an optical oxygen sensor has been investigated [177]. PS composite nanofibers doped with an Eu^{3+} complex were found to exhibit a high sensitivity towards oxygen [178,179].

3.3.3. Inorganic composite fibers

A relatively large number of publications is concerned with ZnO nanofibers and their sensing properties relative to different gases. ZnO nanofibers with an average diameter of 150 nm were reported to exhibit excellent sensing properties against ethanol at an operating temperature of 300 °C, including a rapid response (about 3 s) and recovery (about 8 s) time and a high selectivity [180], ZnO nanofibers to be used in gas sensors for the detection of ethanol were also reported in other publications [181,182]. An enhanced sensitivity of nearly 90% was obtained at low ethanol concentrations of 10 ppm. Solid and hollow ZnO nanofibers were used as acetone detectors [183]. The ZnO hollow nanofibers showed improved response to acetone at 220 °C with good selectivity and stability, which is attributed to the 1D hollow nanostructure. The sensing properties, including high sensitivity, short response and recovery

times of a sensor fabricated from ZnO nanofibers for CO detection was also investigated [184,185]. It was found that the size and crystallinity of grains in individual ZnO nanofibers greatly influence their sensing properties for CO detection. Nanofibers composed of large grains were superior to those of a sensor fabricated with nanofibers with small grains. ZnO nanofibers were also used for humidity detection with the humidity sensing properties of the fiber mats being studied by quartz crystal microbalance measurements [186]. ZnO nanofibers were furthermore employed for the detection of NO_2 [185,187] and they were used to sense glucose [188]. In addition to ZnO nanofibers the preparation and the analysis of sensing properties of SnO_2 nanofibers were reported in a set of publications [189–192]. For these nanofibers sensing applications were directed among others towards hydrogen [190] and NO_2 [191]. Furthermore nanofibers composed of pure TiO_2 were prepared displaying reversible rapid responses and high sensitivities for methanol, moisture [193] as well as NO_2 and CO [194].

In addition to pure ZnO, SnO_2 and TiO_2 corresponding composite nanofibers, doped nanofibers were prepared and their sensing properties were evaluated. Such combinations of nanofibers with other compounds were studied aiming at higher sensitivities and lower driving temperatures. TiO_2–ZnO core–shell nanofibers were prepared via a two-step process in which the TiO_2 core nanofibers were made by electrospinning with the ZnO shell layers subsequently being prepared using a layer deposition [195]. Good sensitivity and dynamic repeatability were observed with respect to oxygen. Co–ZnO composite nanofibers with 0, 0.2, 0.4, and 0.8 wt.% were prepared and it was found that the *m*-xylene sensing properties of the ZnO nanofibers are effectively enhanced via the Co doping with the best sensing properties found for the 0.4 wt.% Co–ZnO composite nanofibers at 320 °C [196]. Humidity sensors based on double-layer ZnO–TiO_2 nanofibers displayed corresponding impedance changes by more than four orders of magnitude within the whole humidity range from about 10 to 95% relative humidity with response and recovery times amounting to about 11 and 7 s, respectively [197,198]. For SnO_2–ZnO core–shell nanofibers it was reported that the sensing properties related to CO were sharply enhanced by forming a ZnO shell layer on the SnO_2 fibers. The enhancement is attributed to the formation of an electronically fully depleted shell layer due to the presence of a heterojunction between the ZnO shell and the SnO_2 core. This fully depleted shell layer is believed to cause strong changes in resistance during adsorption and desorption of gases [199]. Similar arguments were used for SnO_2–ZnO hollow nanofibers exhibiting a considerable sensitivity and good stability against toluene at 190 °C. These features were attributed to the special 1D hollow structure and the promoting effect of the SnO_2/ZnO heterojunction [200]. For Cu-doped ZnO nanofibers it was observed that the H_2S sensing properties are effectively improved by Cu doping [201]. Very effective ethanol sensing was reported for SnO_2/ZnO composite nanofibers [202]. Fe-doped SnO_2 nanofibers were prepared exhibiting a high sensitivity and rapid response/recovery to ethanol at 300 °C [203]. Fe-doped SnO_2 nanofibers can thus be used as the sensing material for fabricating high performance ethanol sensors. Unloaded and Pd-loaded SnO_2 nanofibers were prepared along a new route allowing to suppress grain growth and to tune the sensitivity and selectivity of nanocrystalline fibers [204]. For Pt doped SnO_2 nanofibers it was found that the responses of 0.08 wt% Pt doped SnO_2 nanofibers to 4–20 ppm H_2S, were about 26–40 times higher than those of pure SnO_2 nanofibers [205]. NiO-doped SnO_2 (NSO) nanofibers were shown to exhibit good formaldehyde sensing properties at an operating temperature of 200°, with the minimum-detection-limit down to 0.08 ppm [206]. Core TiO_2/ZnO nanofibers having an average diameter of about 100 nm and a shell of ultrathin PPy layer with a thickness of about 7 nm are reported to exhibit a fast response over a wide dynamic range and a high sensitivity with a detection limit of 60 ppb as NH_3 gas sensor [207]. For TiO_2-Pt hybrid nanofibers it was shown that compared to pristine TiO_2 nanofibers the incorporation of Pt nanoparticles into TiO_2 nanofibers can greatly enhance the oxidation of hydrazine in neutral solution in the amperometric hydrazine sensor [208].

In addition to these ZnO, SnO_2 and TiO_2 based inorganic nanofiber systems a broad spectrum of other types of material has been used to prepare nanofibers targeting sensor application. Highly porous CuO fibers are reported showing a high sensitivity and fast response/recovery towards ethanol vapour [209]. Copper oxide nanofibers prepared by electrospinning and subsequent thermal treatment processes were demonstrated to allow a glucose non-enzymic detection [210]. The sensing properties of sensors fabricated from nanograin CuO nanofibers were studied addressing CO and NO_2 [211]. Importantly, the sensitivity of the sensor containing larger nanograins is much higher than that of the sensor with smaller ones. Pd (IV)-doped CuO oxide composite nanofibers have been successfully employed to construct an amperometric non-enzymic glucose sensor showing excellent selectivity, reproducibility and stability [212]. Cobalt oxide-doped copper oxide composite nanofibers prepared via electrospinning followed by thermal treatment processes have been exploited as active electrode material for a direct enzyme-free fructose detection [213]. Also α-Fe_2O_3 ceramic nanofibers were prepared displaying rapid response-recovery and high sensitivity characteristics with resect to EtOH vapor [214]. N-type Fe_2O_3 nanobelts and P-type $LaFeO_3$ nanobelts were prepared by electrospinning, the evaluation showing that the optimum operating temperature of the gas sensors fabricated from Fe_2O_3 nanobelts is 285 °C, whereas that from the $LaFeO_3$ nanobelts amounts to 170 °C [215]. Highly porous Mn_2O_3-Ag nanofibers were employed for the immobilization matrix for glucose oxidase (GOD) to construct an amperometric glucose biosensor. The biosensor shows fast response to glucose, high sensitivity, low detection limits and excellent selectivity [216]. Mn_2O_3 nanofibers were applied to construct an amperometric sensor for hydrazine detection in neutral phosphate buffer [217]. The hydrazine sensor showed a fast response time (within 5 s), a wide linear range, a high sensitivity, a good limit of detection as well as good reproducibility and selectivity. An impedance-type humidity sensor was fabricated based on the $BaTiO_3$ nanofiber [218,219].

The impedance-type humidity sensor exhibited a fast response/recovery property. A nonenzymic glucose sensor was developed based on Ni nanoparticle-loaded carbon nanofiber paste electrodes [220]. An amperometric nonenzymic glucose sensor based on Au-doped NiO nanobelts has been fabricated and applied successfully to a nonenzymic glucose detection [221]. Also reported in the literature is the simultaneous electrochemical determination of dopamine, uric acid and ascorbic acid using carbon nanofibers modified electrodes loaded with palladium nanoparticles [222,223], Au-loaded In_2O_3 nanofibers-based ethanol micro gas sensors with low power consumption [224], the preparation of polycrystalline tungsten oxide nanofibers for gas-sensing applications [225], C_2H_5OH sensing properties of Zn_2SnO_4 nanofibers [226], improved acetone sensing properties of flat sensors based on Co-SnO_2 composite nanofibers [227], the preparation of $LaFeO_3$ nanofibers by electrospinning for gas sensors with fast response and recovery features [228] the synthesis and gas-sensing characteristics of WO_3 nanofibers via electrospinning [229] and finally the preparation and testing of electrospun gold nanofiber electrodes for biosensors [230].

In conclusion, a richness of highly specific and highly sensitive sensors with fiber-type architectures has been prepared via electrospinning. The fiber systems are based on organic polymer composite as well as inorganic composite materials. Peculiar features which seem to be characteristic of these nanofiber systems include a very high sensitivity and fast response times resulting from the 1-D architecture which make them of immediate interest for technical applications.

3.3.4. Lithium ion batteries

Lithium ion batteries widely used in current consumer electronics are characterized by three primary functional components i.e. anode, cathode and electrolyte designed to control effectively the motion of the ions from the negative electrode to the positive one on discharge and back again on charging.

A set of investigations has been concerned with the preparation of nanofibers, core shell nanofibers to be used as anodes in lithium battery applications. Carbon–cobalt composite nanofibers with diameters ranging from 100 to 300 nm were prepared as anodes by electrospinning and subsequent thermal treatment [231]. These fibers exhibit favourable electrochemical properties with a high reversible capacity of more than 750 mA h g^{-1}. Manganese oxide anode nanofibers based on electrospinning of polymer gels incorporating PMMA and manganese acetate with diameters in the 100–300 nm range were found to be composed of oxide grains with diameters of around 20–25 nm and to display a capacity exceeding 450 mA h g^{-1} on reactions with Li [232]. Carbon-SnO_2 core sheet composite fibers produced via the combination of electrospinning and electrodeposition are reported to possess excellent electrochemical performances when used directly as anode materials [233]. High discharge capacities of about 800 mA h g^{-1} were found for porous SnO_2 nanofibers prepared by electrospinning [234]. These were attributed to the porous nature of the fibers facilitating the diffusion of the liquid electrolyte into the fibers which, in turn, is connected with large volume changes [234]. Recticular tin nanoparticle – dispersed carbon nanofibers originating from appropriately heat treated composite PAN nanofibers were reported to have high charge and discharge capacities amounting to about 800 and 1200 mA h g^{-1} respectively at elevated temperatures of around 800 °C [235]. Nitridated TiO_2 nanofibers and nanotubes were found to display capacities twice as high as the pristine TiO_2 nanostructures [236]. The improvements were attributed to a shorter diffusion length and a higher electronic conductivity along the surface of the nitridated structures. The tin concentration in Sn-carbon nanofibers was found to affect crystal structures and morphologies but also the electrochemical performance significantly with the composition ratios of $SnCl_2$/PAN in the untreated electrospun fibers ranging from 3/3 and 1/1 to 2/3 respectively [237]. Film electrodes composed of electrospun one-dimensional TiO_2 and TiO_2/Ag composite hollow fibers (outer diameter about 1 μm, wall thickness about 200 nm) produced by coaxial electrospinning were successfully applied as anode elements for Li-ion batteries [238]. Here the Ag nanoparticles are homogeneously dispersed in such hollow fibers. The range of further nanofibers structures investigated in the literature for anode applications include $Li_2ZnTi_3O_8$ fibers [239], $LiFePO_4$/carbon composite fibers [240], carbon-tin oxide composite fibers [241], Carbon/SnO_2/carbon/core–shell hybrid nanofibers [242] as well as hollow carbon fibers prepared via coaxial electrospinning of styrene-co-acrylonitrile as core and PAN as shell [243].

Only a few investigations exist on electrospun nanofibers for cathode applications in Li-ion batteries. Long hierarchical vanadium oxide nanowires with diameters in the range of 100–200 nm, a length of up to several millimeters and characterized by the attachment of vanadium oxide nanorods of diameters around 50 nm and a length of 100 nm were prepared by electrospinning combined with annealing processes [244]. The discharge capacity was reported to be in the range from 390 and 200 mA h g^{-1}. One-dimensional (1D) vanadium pentoxide (V_2O_5) nanofibers were synthesized by electrospinning vanadium sol–gel precursors containing vanadyl acetylacetonate and PVP followed by sintering [245]. Single-phase electrospun nanofibers with 300–800 nm in diameter and 20–50 μm in length were obtained. Furthermore mesoporous V_2O_5 nanofibers were fabricated by combining sol–gel processing with electrospinning followed by annealing in air [246]. The resulting nanofibers were about 350 nm in diameter and consisted of porous polycrystalline vanadium oxide with a specific surface area of around 97 m^2 g^{-1}. The mesoporous nanofibers showed a significantly enhanced Li ion storage capacity of 370 mA h g^{-1} and above and a high charge/discharge rate of up to 800 mA g^{-1} with only small cyclic degradation

Finally electrospinning has been employed to produce highly porous polymer membranes to become activated with liquid electrolytes for application in Li-ion batteries. One polymer which has been used in several investigations is poly (vinylidene fluoride-co-hexafluoropropylene) [247–250]. A fully-interconnected porous structure – porosity up to 87% – of the host polymer membrane was prepared by electrospinning

allowing a high electrolyte uptake—up to 550–600% and an enhanced ionic conductivity. Polymer electrolytes were prepared by activating the membrane with liquid electrolytes such as 1 M $LiPF_6$ in ethylene carbonate (EC)/dimethyl carbonate (DMC) [249] or 1-butyl-3-methylimidazolium bis(trifluoromethanesulfonylimide) [250]. Furthermore PAN has been used in the preparation of such membranes [251–255] combined in some cases with lithium aluminum titanium phosphate [254] or lithium lanthanum titanate oxide particles [255] in composite fibers. Typically nanofiber diameters around 300–400 nm were prepared. The membranes displayed a good mechanical strength and significant porosity and exhibited a high uptake when activated with liquid electrolytes such as 1 M lithium hexafluorophosphate ($LiPF_6$) in a mixture of organic solvents including ethylene carbonate (EC)/ethyl methyl carbonate (EMC) [252,255]. Other investigations published in the literature were concerned with membranes based on PVDF [256] as well as blends of PVDF with poly(vinylchloride) (PVC) [257]. In the latter case it was found that both electrolyte uptake and ionic conductivity of the composite polymer electrolytes increased with the addition of PVC. Finally membranes of composites of thermoplastic polyurethane (TPU) with different amounts of PVDF (80, 50 and 20 wt.%) are prepared by electrospinning with polymer electrolytes and being activated with 1 M $LiClO_4$/ethylene carbonate/propylene carbonate [258].

3.3.5. Fuel cells

Fuel cells converting the chemical energy from a fuel into electricity through a chemical reaction with oxygen or other oxidizing agents contain three principal building blocks which are sandwiched together: the anode, the electrolyte, and the cathode. At the anode a catalyst has to oxidize the fuel turning it into a positively charged ion and a negatively charged electron. Hydrogen is the most common fuel, but hydrocarbons such as natural gas and alcohols like methanol are also used. The electrolyte has to be designed so that ions can pass through it but the electrons cannot. Frequently it is a proton-conducting polymer membrane separating the anode and cathode sides. The freed electrons have to travel through a wire creating thus electric current. At the cathode, the ions have to be reunited with the electrons and the two react with a third chemical, often oxygen, to create, for instance, water or carbon dioxide. A typical fuel cell produces a voltage from 0.6 to 0.7 V at full rated load. As far as electrospun nanofibers are concerned they have been designed to work either as proton conductive membranes, as anodes or also cathodes.

Composite proton exchange membranes produced via electrospinning of nanofibers tend to consist of Nafion as one of the components. Nafion is a sulfonated tetrafluoroethylene based fluoropolymer–copolymer with ionic properties i.e. it is an ionomer [259–264]. Nafion has the advantage of displaying excellent thermal and mechanical stabilities. The composite membranes prepared by electrospinning are in most cases nonwovens composed of polymers such as PVA, partially sulfonated poly (ether sulfone), sulfonated polystyrene, poly(phenyl sulfone) or inorganic materials such as sulfated zirkonia (S-ZrO_2) with Nafion subsequently being forced to infiltrate the pores of the nonwoven. The resulting composite membranes have in general higher proton conductivities than pure Nafion membranes with the conductivities being dependent on the fiber diameters. The assumption is that the fiber/Nafion interfaces form continuous pathways for proton transport.

To obtain composite membranes Nafion and poly(phenylen sulfone) were simultaneously electrospun into a dual-fiber mat [259]. Two distinct membrane structures characterized either by Nafion being reinforced by a poly (phenylen sulfone) nanofiber network or by Nafion nanofibers being embedded in inert/uncharged poly(phenylene sulfone) nanofiber networks were subsequently produced by follow-on processing. Also partially sulfonated poly (ether sulfone) was electrospun to bead-free nanofibers and the porous nanofibrous membranes were impregnated with appropriate amounts of Nafion solution [260]. An excess amount of Nafion solution was used in this approach to form a uniform top layer. The sulfonation has been observed to lead to a considerable decrease in nanofiber diameters and to a narrower diameter distribution. Another type of hybrid proton exchange membrane was fabricated by incorporating sulfonated polystyrene electrospun fibers into Nafion [261]. With the introduction of such fibers a large amount of sulfonic acid groups were observed in Nafion to aggregate onto the interfaces between the fibers and the ionomer matrix, forming continuous pathways for facile proton transport. The resulting hybrid membranes had higher proton conductivities than those of recast Nafion, and the conductivities were controlled by selectively adjusting the fiber diameters. The preparation of composite membranes via electrospinning of aqueous solutions of PVA with thicknesses around 19–97 μm containing Nafion infiltrated into a porous membrane has been the focus of two publications [262,263]. The fibers tend to have diameters around 200–300 nm, they were functionalized on their external surface with sulfonic acid groups in order to contribute in the proton conduction of Nafion [262]. The proton conduction of such a composite membrane (47 μm thick) as determined by impedance spectroscopy approached 0.022 S/cm at 70°. For such Nafion/PVA composite membranes the resistance to methanol permeation showed a linear variation with the thickness. A rather different type of hybrid membrane has also been reported being fabricated by incorporating superacidic sulfated zirconia (S-ZrO_2) fibers into recast Nafion [264]. Due to the introduction of electrospun superacidic fiber mats, a large amount of protogenic groups was observed to aggregate in the interfacial region between S-ZrO_2 fibers and the ionomer matrix, forming continuous pathways for proton transport. The resulting hybrid membranes displayed high proton conductivities, which could be controlled by selectively adjusting the fiber diameters and fiber volume fraction.

Coming to anode elements in fuel cells the development of a solid oxide fuel cell anode by impregnating catalytic Ni and Ni-CeO_2 nano-particles on 8YSZ fiber structure (Yttria Stabilized Zirconia) was reported [265]. Nano-scalar 8YSZ fibers were successfully fabricated by electrospinning and were well matched with the 8YSZ electrolyte. An alternative route to fabricate nanofiber-derived low-Ni-content

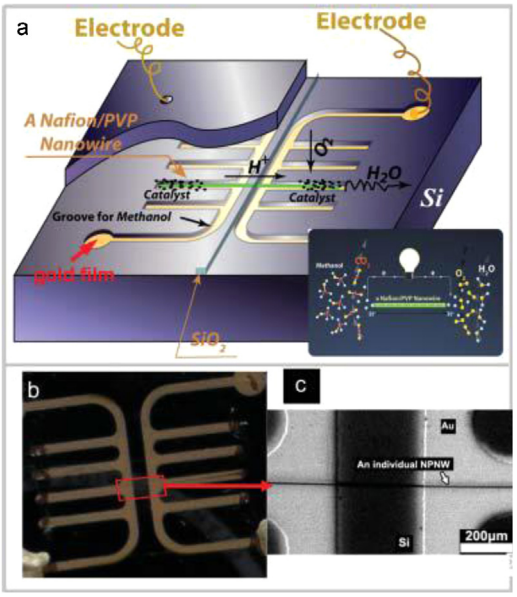

Fig. 7. (a) Schematic 3D representation of the structure of the micro fuel cell. A groove in the Si substrate (with a 50 nm Au film deposited on the groove) serves simultaneously as "microchannel" fuel container and an electrode. The nanowires were kept in place on the Si substrate by mounting a silicon oxide "dam" (of 100 mm width and several mm thickness) on top in the middle of the silicon substrate. The inset shows the working principle of the micro-fuel cell. (b) A top-view (overhead view) of the micro fuel cell. (c) A magnified image of the area marked by the red rectangle in (b). Reprinted with permission from ref. [269]. Copyright (2008) WILEY-VCH Verlag GmbH & Co. KGaA, Weinheim.

anodes for solid oxide fuel cells has also been reported [266]. Here uniform YSZ nanofibers were first prepared by electrospinning of 8YSZ dispersions; the fiber surfaces were then electrolessly plated with a layer of Ni after sintering of the electrospun fibers. The deposited anode had a Ni loading of 30%, a value well below the conventional percolation threshold.

Refering finally to cathodes Yttria stabilized zirconia (YSZ) and $La_{0.8}Sr_{0.2}MnO_3$ (LSM) nanofibers were prepared with diameters of the nanofibers from around 200 nm up to tens of microns [267]. These nanofibers exhibit a high chemical and structural stability at high temperatures. The results indicate that these nanostructures are promising materials for fabricating high performance solid oxide fuel cell cathode. Furthermore Perovskite-type $Ba_{0.5}Sr_{0.5}Co_{0.2}Fe_{0.8}O_{3-\delta}$ (BSCF) nanofibers were prepared via electrospinning as a cathode for intermediate temperature solid oxide fuel cells [268]. BSCF nanofibers were prepared by treating electrospun poly(vinyl pyrrolidon)/$Ba_{0.5}Sr_{0.5}Co_{0.8}Fe_{0.2}O_{3-\delta}$ composite fibers at high temperatures in an air atmosphere.

Finally a micrometer-sized fuel cell based on Nafion/PVP nanowires as the electrolyte has been presented in the literature as depicted in Fig. 7 [269]. The "micro fuel cell" was monolithically integrated on a silicon substrate and consisted of the nanowires, PtRu/C and Pt/C catalysts, two outleading electrodes, methanol as fuel, and air as oxidant. The performance of the micro fuel cell was reported to be orders of magnitude higher than that of a traditional fuel cell power source. The micro fuel cell generated a 314 mV open-circuit voltage (OCV), a maximum I_d of about 1.21 mA/mm^2 (at zero applied load), and a maximum P_n of about 0.095 mW/mm^2 at room temperature. It was found that the performance of the micro fuel cell improved dramatically with increasing temperature. The performance of the micro fuel cell at 333 K reveals an increase of the OCV of over 100 mV. The maximum I_d (at zero applied load) increased by a factor of three and the maximum P_n amounted to 0.348 mW/mm^2. The designed micro fuel cell is claimed to allow the use of different fuels and oxidants. Finally, the power generated by a single 2.1 mm nanowire-based micro fuel cell was found to be about 1.54 mW.

The use of electrospun 3D carbon fiber electrodes also enhanced the efficiency of microbial fuel cells significantly. The higest ever bioelectrocatalytic anode current density of up to 30 A m^{-2} was shown using porous carbon fiber mats produced by gas-assisted electrospinning at very low specific weight (42 g/m^2) [270].

These results reported above make it obvious that electrospun nanofibers of various compositions are attractive candidates for the construction of lithium ion batteries acting as anodes, cathodes or also of polymer membranes to become activated with lithium electrolytes. A high electroyte uptake or a high discharge capability seem to be features related to the highly porous nature of the nanofiber arrangements.

3.3.6. Solar cells

Electrospinning investigations focusing on solar cells have primarily dealt with dye-sensitized ones (DSSCs) considered to be extremely promising because of their high efficiency and low production costs. In such dye-sensitized cells photosensitizers absorb light to generate excited electron–hole pairs which next undergo interfacial charge separation. The electrons then propagate through the photoelectrode while the holes diffuse through an electrolyte solution to the counter electrode. Charge collection tends to compete with charge recombination happening at the interfaces of photoelectrode/dye/electrolyte. To realize high device efficiencies, charge diffusion must be enhanced while minimizing charge recombination. One-dimensional (1D) nanostructures (e.g., nanowires, nanorods, nanotubes, nanobelts, cauliflower-shaped structures) are expected to have superior electron transport characteristics compared to conventional NP-based because the relatively low electronic junction densities found in 1D nanostructures.

In the case of the most frequently used TiO_2 photoelectrodes the effect of parameters such as morphology, pore volume, the crystallinity of TiO_2 as well as of doping on charge transport and recombination processes have been evaluated in a set of papers [271–281]. To prepare dye-sensitized solar cells with high energy conversion efficiencies TiO_2 nanorods were electrospun from a solution of titanium *n*-propoxide and poly(vinyl acetate) in dimethyl formamide [271]. Investigation disclosed that the efficiency of the DSSCs can be enhanced by optimizing the nanorod morphology to facilitate charge transport. The prepared nanorods had an intrinsically higher sensitizer loading capability than conventional TiO_2 nanoparticles and longer electron lifetimes. This provides an enhanced

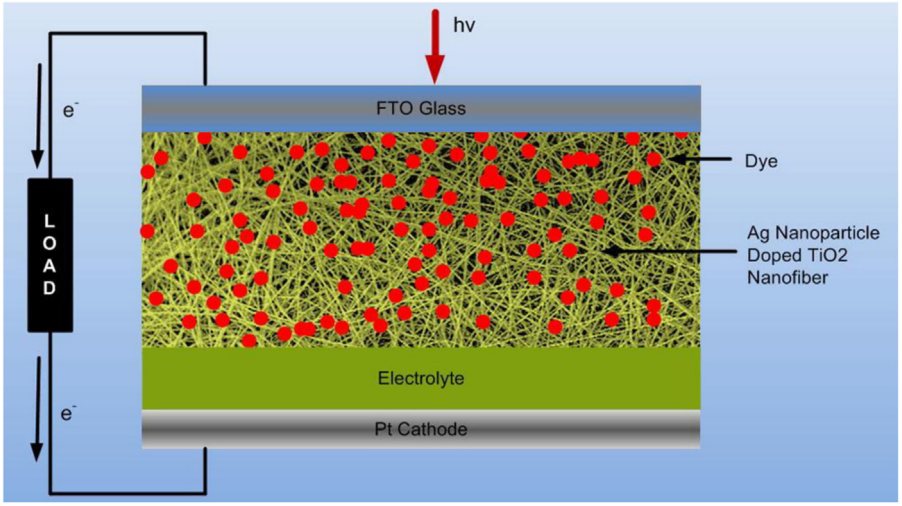

Fig. 8. Schematic diagram of DSSC based on Ag nanoparticle doped TiO_2 nanofiber. Reprinted with permission from ref. [279]. Copyright (2011) Elsevier B.V.

effective photocarrier collection as well as enhanced conversion efficiency. A low-cost fabrication of TiO_2 nanorod photoelectrodes for dye-sensitized solar cell application has been based on electrospinning with PEO as excellent matrix polymer owing to its low decomposition temperature, wide availability, and environmental friendliness [272]. To obtain rutile titania (TiO_2) nanofibers and nanorods a polymeric solution containing a titanium precursor and PVP in acetic acid–ethanol mixtures was electrospun to fibers which were subsequently sintered at 800 °C [273]. The resulting continuous, polycrystalline porous fibers which were found to contain TiO_2 grains with sizes in the range 15–20 nm were broken down into nanorods by mechanical grinding. A composite made of electrospun TiO_2 nanofibers and conventional TiO_2 nanoparticles has been reported to be characterized by a significant improvement of the harvesting of light without substantially sacrificing the attachment (uptake) of dye molecules yielding thus dye-sensitized solar cells with significantly improved efficiency [274]. Anatase mesoporous TiO_2 nanofibers were prepared for solid-state dye-sensitized solar cells with high surface areas of up to 112 $m^2\,g^{-1}$ enhancing the dye uptake considerably [275]. A further paper provides a simple recipe for the fabrication of electrospun TiO_2 nanorod-based efficient dye-sensitized solar cell using a Pechini-type solution [276]. The Pechini-type solution of TiO_2 nanofibers produced a highly porous and compact layer of TiO_2 upon doctor-blading and sintering without the need for an adhesion and scattering layers or $TiCl_4$ treatment. Higher performance is expected in electronic devices that utilize metal oxide semiconductors in vertical architecture owing to the direct and effective electron transport. The production of anatase phase vertical TiO_2 nanowires on conductive substrates has been demonstrated [277]. Reported is not only the facile fabrication of vertical arrays of anatase TiO_2 nanowires but also of corresponding wires using electrospinning. At first aligned nanofibrous TiO_2 ribbons were produced and then assembled to vertical nanowires. Quantum dot (QDs) decorated TiO_2 nanofibrous electrodes, unlike organic dye sensitizers able to yield multiple carrier generations due to the quantum confinement effect, have also been prepared [278]. Reported are first attempts to combine these two novel approaches, in which CdS (size about 18 nm) and CdSe (size about 8 nm) QDs were placed onto electrospun TiO_2 nanofibrous (diameter about 80–100 nm) electrodes. Silver nanoparticle doped TiO_2 nanofibers prepared by the electrospinning process were used as the photoanode to fabricate dye sensitized solar cells (Fig. 8) [279].

It was found that the nanoparticle doped solar cells have a significantly increased photocurrent density resulting in a 25% improved conversion efficiency compared to undoped solar cells. The improved performance is attributed to two factors i.e. the increased light harvesting efficiency due to the plasmon enhanced optical absorption induced by Ag nanoparticles, and the improved electron collection efficiency as a result of faster electron transport in the Ag doped TiO_2 nanofiber photoanode. With the aim to improve the performance of dye sensitized solar cells, to control the electron transport properties to harvest and collect effectively photogenerated electrons a bilayer TiO_2 nanofiber photoanode was investigated. This combined both smaller and larger-diameter TiO_2 nanofibers readily available by a one step nozzleless electrospinning technique [280]. The photoanode consisted of two layers of TiO_2 nanofibers with different diameters i.e. 60 and 100 nm, respectively. The smaller-diameter nanofiber layer with a high surface-to-volume ratio was used to adsorb dye molecules in sufficient quantities and to directly transport electrons released from excited dyes. On the other hand, the layer composed of nanofibers with larger diameters worked as light scattering element (i.e. it extends the light path in the devices), adsorbed sufficient dye molecules for energy harvest, and provided higher pore volume to facilitate electrolyte diffusion for regenerating sensitized dye molecules in the photoanode. The power conversion efficiency of the solar cell could be improved by 17% for the bilayer of TiO_2 nanofiber photoanode.

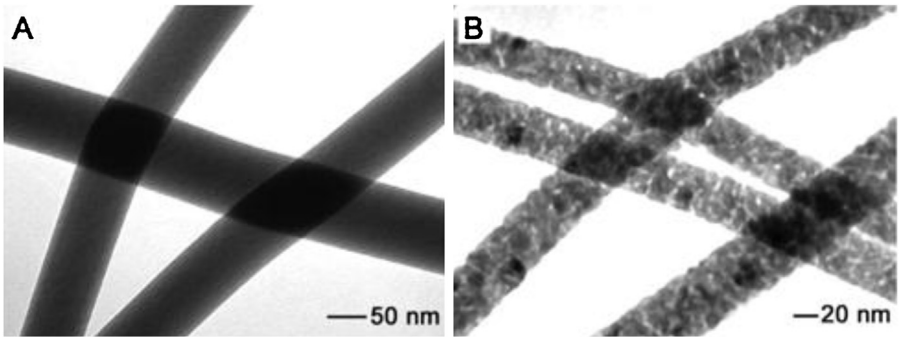

Fig. 9. (A) TEM image of TiO_2/PVP composite nanofibers fabricated by electrospinning; (B) TEM image of the same sample after it had been calcined in air at 500 °C for 3 h. Reprinted with permission from ref. [286]. Copyright 2003 American Chemical Society.

To prepare dye-sensitized solar cells with electrospun poly (vinyl alcohol) (PVA) nanofibers containing Ag nanoparticles were prepared by electrospinning using a PVA solution containing silver nitrate (AgNO3) [281]. The electrospun PVA nanofibers containing $AgNO_3$ were irradiated for this purpose with UV light at 310–380 nm to generate Ag nanoparticles within the nanofibers. Recognizing the fact that the application of electrospun nanofibers in electronic devices is limited due to their poor adhesion to conductive substrates efforts were made to improve this via a seed layer introduced on the substrate prior to the deposition of the electrospun composite nanofibers [282]. Such seed layers were found to facilitate the release of interfacial tensile stress during calcination and to enhance the interfacial adhesion of the Al-doped ZnO (AZO) nanofiber films grown on fluorine-doped tin oxide (FTO) substrates [282]. Dye-sensitized solar cells based on these nanofiber photoelectrodes were fabricated and investigated. An energy conversion efficiency (η) of 0.54–0.55% was obtained under irradiation of simulated sunlight (100 mW/cm^2) indicating a massive improvement of the efficiency in the AZO nanofiber film. Also flower shaped nanostructures of a transparent conducting oxide, SnO_2, have been reported to be produced by an electrospinning technique via precisely controlling the precursor concentration in a polymeric solution [283]. The flower structures were made up of nanofibrils of diameters ranging from 70 to 100 nm, which in turn consisted of linear arrays of single crystal nanoparticles with sizes in the range from 20 to 30 nm. It is claimed that high performance dye-sensitized solar cells with record open circuit voltage result from using such tin oxide nanoflower structures. Finally electrospun carbon nanofibers have been explored as an electrocatalyst and low-cost alternative to platinum for triiodide reduction in dye-sensitized solar cells [284]. The results of electrochemical impedance spectroscopy and cyclic voltammetry measurements have indicated that the carbon nanofiber based counter electrodes exhibit low charge-transfer resistance, large capacitance, and fast reaction rates for triiodide reduction.

So in conclusion, nanofibers as produced by electrospinning offer a set of benefits for applications in solar cells. They may improve, for instance, the performance of dye sensitized solar cells by an enhanced electron collection efficiency—as a result of faster electron transport in nanofiber photoanodes. Also, layer composed of nanofibers may act efficiently as light scattering element extending the light path in the devices and provide high pore volumes to facilitate electrolyte diffusion for regenerating sensitized dye molecules in the photoanode. Modifications of the fiber topologies – taking flower structures as an example – offer further routes towards better performances.

3.3.7. *Nanofibers in photocatalytic applications*

Titanium dioxide (TiO_2) is one of the most frequently studied semiconductor photocatalysts. The photocatalytic efficiency is known to be dependent upon the surface area (morphology) and the specific type of crystal phase. Nanoparticles (with increased surface-to-volume ratio) and anatase or a mixture of phases like anatase and rutile, respectively provide the most active catalytic response. The agglomeration and the separation of TiO_2 particles after catalytic reations are existing challenges. Electrospun nanofibers with high surface areas and porosities provide an effective support for photocatalytic active TiO_2 nanoparticles. The TiO_2 immobilised polymeric nanofibers can easily be made by the process of electrospinng using a template polymer solution together with either titanium salt ot pre-made TiO_2 nanoparticles with subsequent post annealing and calcinations steps [285,286]. The TiO_2

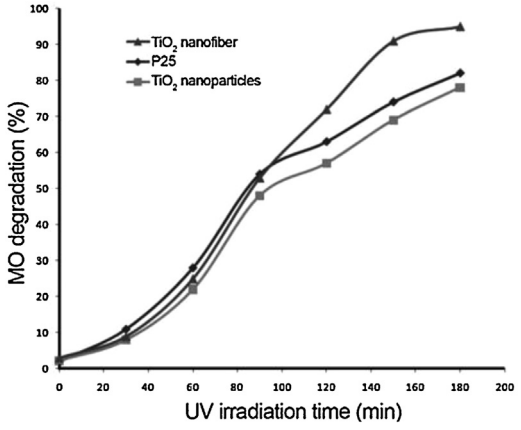

Fig. 10. Photocatalytic degradation of methyl orange (MO) by TiO_2 nanomaterials. Reprinted with permission from ref. [289]. Copyright 2011 Science+Business Media.

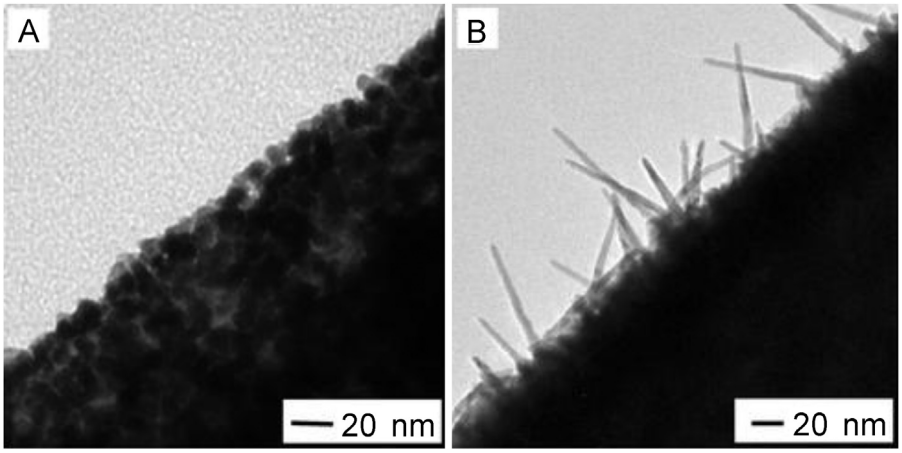

Fig. 11. TEM images of (A) the edge of an anatase nanofiber after it had been decorated with Pt nanoparticles; (B) the same sample after the surface had been decorated with Pt nanoparticles, followed by growth of Pt nanowires in another polyol reduction bath for 13.5 h; Reprinted with permission from ref. [293]. Copyright (2008) American Chemical Society.

nanopartciles can also be immobilized on the surface of electrospun nanomats in a post electrospinning functionalisation step (Fig. 9).

For example, TiO_2 nanoparticles were immobilized on the surface of a flouoropolymer nanomat by making a complex between Ti ions and carboxyl group on fluoropolymer species followed by hydrothermal precipitation [287]. In one of these studies, the photocatalytic efficiency of the anatase TiO_2 nanofiber membrane was found to amount to 72%, which is significantly superior to that of anatase TiO_2 thin films (44%) [288]. The use of hybrid nanofibers (poly (vinyl acetate) (PVAc)/TiO_2) was demonstrated by Jabbari et al. for the photocatalytic degradation of methyl orange. The TiO_2 electrospun hybrid fibers showed efficient photooxidative decomposition of methyl orange in comparison to TiO_2 nanoparticles (Fig. 10) [289].

Hierarchial structures composed of rutile TiO_2 nanorods on anatase TiO_2 nanofibers and characterized by a three dimensional high surface area (20.41 $m^2\,g^{-1}$) were proved to be superior in photocatalytic activity in comparison the pure anatase TiO_2 nanofibers [290]. The degradation of the dye Rhodamine 6G was taken as the example for photodegaradtion studies. A combination of features such as high surface areas, a fast charge separation and fast diffusion rates between photoexcited electrons and holes originating from the 1D exposed single crystal surface of rutile nanorods were given as reasons for increased photocatalytic activities.

The photocatalytic reaction involves production of photoexcited electrons and positively charged holes. The photocatalytic activity is dependent upon charge separation, charge transport to the surface and recombination of charges. Shifting of Fermi level of titanium to more negative potential could prevent the recombination of excited electrons and holes thereby increasing the efficiency of photocatalysis. This could be done via additives i.e. by attaching other metal particles to TiO_2. This concept of improved photocatalytic efficiency was demonstrated for many different metal nanopartcles including Au, Ag, Pt, Rh, V and W-doped TiO_2 electrospun nanofibers (Fig. 11) [291–295].

The enhanced photocatalytic properties of hybrid nanofiber mats of anatase TiO_2 nanoparticles and multi-walled carbon nanotubes (MWNTs) were also reported in the literature. The presence of MWNTs prevents agglomeration of TiO_2 naoparticles, increases the surface area and minimizes the chance of e^-/h^+ pair recombination [296].

Liu et al. designed a bicomponent nanofiber photocatalyst consisting of TiO_2 and SnO_2 semiconductors by the process of side-by-side electrospinning. This morphology provides the advantage of maximum exposure of both of the two components to the surface. The photogenerated electrons in the TiO_2/SnO_2 system accumulate on SnO_2 and holes accumulate on TiO_2. The side-by-side heterojunction structure obviously promotes an increase in the charge separation of the photogenerated electrons and holes thus increasing the quantum efficiency [297]. There are furthermore some scattered studies regarding the use of other electrospun semiconductor oxides including BiOCl, Bi_2O_3, ZnO nanomats for photocatayltic applications [298–300].

The results reported above demonstrate clearly that electrospun nanofibers can be designed as highly active photocatalytic systems owing their impressive features to a major extent to their high surface areas and porosities. They may also provide an effective support for photocatalytic active nanoparticles. Modifications allowing to enhance the catalytic activity may include composite formation as well as the formation of various types of hierarchical structures. A lot of progress can be expected in this area in the near future.

4. Conclusions

Electrospinning has succeeded within the last years in establishing itself as an internationally highly recognized enabeling method granting access to a broad range of one-dimensional functional nanoobjects including nanofibers, nanorods as well as nanotubes. The unique features which

make nanofibers/nanotubes and nonwovens composed of them of interest both for fundamental studies as well as for applications are the 1D-confinements present, the high orientations of structural elements induced along the fibers via electrospinning, strongly restricted material and electronic diffusion distances perpendicular to the fiber axis, high surface area as well as the high porosities of up to 90% observed for the corresponding electrospun nonwovens. Significant progress has recently been made not only in the fundamental understanding and modeling of the details of the complex processes governing fiber formation but also in the development of a broad range of technical spinning devices. One area which has gained strong benefits from such developments is Life Science with tissue engineering, drug delivery, wound healing being characteristics targets. In view of several review articles published recently in this area this topic has not been included in the present progress report. Future research will proceed in the area of controlled 3D arrangements of electrospun nanofibers and their controlled movement.

As far as technical areas are concerned the impressive progress achieved in basic knowledge on electrospinning and on novel technical realizations has made it possible to extend the range of materials from which one dimensional nanoobjects can be spun in a highly controlled way from conventional synthetic and natural polymers to functional polymers, metals, metal oxides, semiconductor materials, ceramics, rare earth compounds of complex composition all the way towards composites composed of organic and inorganic materials. Nanofibers composed of such materials can today be designed in a highly controlled way to display specific structural features including various types of phase morphologies and surface topologies as well as to show unique functions including in particular magnetic, optical, electronic, sensoric, catalytic functions specific for one-dimensional architectures. Impressive developments have also been achieved towards the exploitation of such functional nanofibers in technical applications involving among others fuel cells, lithium ion batteries, solar cell, electronic sensors as well as photocatalysts. One major highly ambitious target is currently the incorporation of such functional nanofibers in micrometer-sized electronic devices or even the construction of such devices purely from nanofibers. Electrospinning can without any doubt be expected to contribute greatly to further advances in nanotechnology.

References

[1] Huang ZM, Zhang YZ, Kotaki M, Ramakrishna S. A review on polymer nanofibers by electrospinning and their applications in nanocomposites. Composites Science and Technology 2003;63:2223–53.

[2] Dersch R, Greiner A, Wendorff JH. Polymer nanofibers by electrospinning. In: Schwartz JA, Contesen CJ, Putger K, editors. Dekker encyclopedia of nanoscience and nanotechnology. New York: Marcel Dekker; 2004. p. 2931–8.

[3] Li D, Xia Y. Electrospinning of nanofibers: Reinventing the wheel? Advanced Materials 2004;16:1151–70.

[4] Greiner A, Wendorff JH. Electrospinning: A fascinating method for the preparation of ultrathin fibers. Angewandte Chemie International Edition 2007;119:5670–703.

[5] Reneker DH, Yarin AL, Zussman E, Xu H. Electrospinning of nanofibers from polymer solutions and melts. Advances in Applied Mechanics 2007;41:43–195.

[6] Greiner A, Wendorff JH. Functional self-assembled nanofibers by electrospinning. Advances in Polymer Science 2008;219:107–71.

[7] Wendorff JH, Agarwal S, Greiner A. Electrospinning: Materials, processing and applications. Weinheim: Wiley-VCH; 2012, 254 pp.

[8] Agarwal S, Wendorff JH, Greiner A. Use of electrospinning technique for biomedical applications. Polymer 2008;49:5603–21.

[9] Sill TJ, von Recum HA. Electrospinning applications in drug delivery and tissue engineering. Biomaterials 2008;29:1989–2006.

[10] Kanani AG, Bahrami SH. Review on electrospun nanofibers scaffold and biomedical applications. Trends in Biomaterials & Artificial Organs 2010;24:93–115.

[11] Dotti F, Varesano A, Montarsolo A, Aluigi A, Tonin C, Mazzuchetti G. Electrospun porous mats for high efficiency filtration. Journal of Industrial Textiles 2007;37:151–62.

[12] Balamurugan R, Sundarrajan S, Ramakrishna S. Recent trends in nanofibrous membranes and their suitability for air and water filtrations. Membranes 2011;1:232–48.

[13] Zucchelli A, Focarete ML, Gualandi C, Ramakrishna S. Electrospun nanofibers for enhancing structural performance of composite materials. Polymers for Advanced Technologies 2011;22:339–49.

[14] Jiang S, Duan G, Hou H, Greiner A, Agarwal S. Novel layer-by-layer procedure for making nanofiber reinforced high strength, tough, and transparent thermoplastic polyurethane composites. ACS Applied Materials & Interfaces 2012;4:4366–72.

[15] Earnshaw S. On the nature of the molecular forces which regulate the constitution of the luminiferous ether. Transactions of Cambridge Philosophical Society 1842;7:97–112.

[16] Reneker DH, Yarin AL, Fong H, Koombhongse S. Bending instability of electrically charged liquid jets of polymer solutions in electrospinning. Journal of Applied Physics 2000;87:4531–47.

[17] Yarin AL, Koombhongse S, Reneker DH. Taylor cone and jetting from liquid droplets in electrospinning of nanofibers. Journal of Applied Physics 2001;90:4836–46.

[18] Yarin AL, Koombhongse S, Reneker DH. Bending instability in electrospinning of nanofibers. Journal of Applied Physics 2001;89:3018–26.

[19] Reznik SN, Yarin AL, Theron A, Zussman E. Transient and steady shapes of droplets attached to the surface in a strong field. Journal of Fluid Mechanics 2004;516:349–77.

[20] Yarin AL, Kataphinan W, Reneker DH. Branching in electrospinning of nanofibers. Journal of Applied Physics 2005;98:064501/1–64501.

[21] Reneker DH, Yarin AL. Electrospinning jets and polymer nanofibers. Polymer 2008;49:2387–425.

[22] Hohman MM, Shin M, Rutledge G, Brenner MP. Electrospinning and electrically forced jets: I: Stability theory. Physics of Fluids 2001;13:2201–20.

[23] Hohman MM, Shin M, Rutledge G, Brenner MP. Electrospinning and electrically forced jets: II Applications. Physics of Fluids 2001;13:2221–36.

[24] Shin YM, Hohmann MM, Brenner MP, Rutledge GC. Experimental characterization of electrospinning: the electrically forced jet and instabilities. Polymer 2001;42:9955–67.

[25] Fridrikh SV, Yu JH, Brenner MP, Rutledge GC. Controlling the fiber diameter during electrospinning. Physical Review Letters 2003;90:144502/1–144502.

[26] Zhou Z, Wu XF, Gao X, Jiang L, Zhao Y, Fong H. Parameter dependence of conic angle of nanofibres during electrospinning. Journal of Physics D 2011;44:435401/1–435401.

[27] Holzmeister A, Yarin AL, Wendorff JH. Barb formation in electrospinning: Experimental and theoretical investigations. Polymer 2010;51:2769–78.

[28] Katti DS, Robinson KW, Ko FK, Laurencin CT. Bioresorbable nanofiber based systems for wound healing and drug delivery: optimization of fabrication parameters. Journal of Biomedical Materials Research B 2004;70:286–96.

[29] Fong H, Chun I, Reneker DH. Beaded nanofibers formed during electrospinning. Polymer 1999;40:4585–92.

[30] Zuo W, Zhu M, Yang W, Yu H, Chen Y, Zhang Y. Experimental study on relationship between jet instability and formation of beaded fibers during electrospinning. Polymer Engineering & Science 2005;45:704–9.

[31] Jarusuwannapoom T, Hongrojjanawiwat W, Jitjaicham S, Wannatong L, Nithitanakul M, Pattamaprom C, Koombhongse P, Rangkupan R, Supaphol P. Effect of solvents on electrospinnability of polystyrene solutions and morphological appearance of

resulting electrospun polystyrene fibers. European Polymer Journal 2005;41:409–21.
[32] Arayanarakul K, Choktaweesap N, Aht-Ong D, Meechaisue C, Supaphol P. Effects of poly(ethylene glycol), inorganic salt, sodium dodecyl sulfate, and solvent system on electrospinning of poly(ethylene oxide). Macromoleculars Materials and Engineering 2006;291:581–91.
[33] Yu JH, Fridrikh SV, Rutledge GC. The role of elasticity in the formation of electrospun fibers. Polymer 2006;47:4789–97.
[34] Deitzel JM, Kleinmeyer JD, Harris D, Tan NCB. The effect of processing variables on the morphology of electrospun nanofibers and textiles. Polymer 2001;42:261–72.
[35] SonWK, Youk JH, Lee TS, Park WH. The effects of solution properties and polyelectrolyte on electrospinning of ultrafine poly(ethylene oxide) fibers. Polymer 2004;45:2959–66.
[36] Chase GG, Reneker DH. Nanofibers in filter media. Journal of Fluid/Particle Separation 2004;16:105–17.
[37] Doshi J, Reneker DH. Electrospinning process and applications of electrospun fibers. Journal of Electrostatics 1995;35:151–60.
[38] Supaphol P, Mit-uppatham C, Nithitanakul M. Ultrafine electrospun polyamide-6 fibers: effect of emitting electrode polarity on morphology and average fiber diameter. Journal of Polymer Science Part B Polymer Physics 2005;43:3699–712.
[39] Mituppatham C, Nithitanakul M, Supaphol P. Effects of solution concentration, emitting electrode polarity, solvent type, and salt addition on electrospun polyamide-6 fibers: a preliminary report. Macromolecular Symposia 2004;216:293–9.
[40] Wannatong L, Sirivat A, Supaphol P. Effects of solvents on electrospun polymeric fibers: preliminary study on polystyrene. Polymer International 2004;53:1851–9.
[41] Beachley V, Wen X. Effect of electrospinning parameters on the nanofiber diameter and length. Material Science Engineering C 2009;29:663–8.
[42] Theron S, Zussman E, Yarin AL. Experimental investigation of the governing parameters in the electrospinning of polymer solutions. Polymer 2004;45:2017–30.
[43] Yang Q, Li Z, Hong Y, Zhao Y, Qiu S, Wang C, Wei Y. Influence of solvents on the formation of ultrathin uniform poly(vinyl pyrrolidone) nanofibers with electrospinning. Journal of Polymer Science Part B Polymer Physics 2004;42:3721–6.
[44] Gupta P, Elkins C, Long TE, Wilkes GL. Electrospinning of linear homopolymers of poly(methyl methacrylate): exploring relationships between fiber formation, viscosity, molecular weight and concentration in a good solvent. Polymer 2005;46:4799–810.
[45] Samatham R, Kim KJ. Electric current as a control variable in the electrospinning process. Polymer Engineering & Science 2006;46:954–9.
[46] Luo CJ, Nangrejo M, Edirisinghe M. A novel method of selecting solvents for polymer electrospinning. Polymer 2010;51: 1654–62.
[47] Qin XH, Yang EL, Li N, Wang SY. Effect of different salts on electrospinning of polyacrylonitrile (PAN) polymer solution. Journal of Applied Polymer Science 2007;103:3865–70.
[48] Uyar T, Besenbacher F. Electrospinning of uniform polystyrene fibers: The effect of solvent conductivity. Polymer 2008;49: 5336–43.
[49] Liu Y, He JH, Yu JY, Zeng HM. Controlling numbers and sizes of beads in electrospun nanofibers. Polymer International 2008;57: 632–6.
[50] Gu SY, Ren J, Vancso GJ. Process optimization and empirical modeling for electrospun polyacrylonitrile (PAN) nanofiber precursor of carbon nanofibers. European Polymer Journal 2005;41:2559–68.
[51] De Vrieze S, Van Camp T, Nelvig A, Hagström B, Westbroek P, De Clerck K. The effect of temperature and humidity on electrospinning. Journal of Material Science 2009;44:1357–62.
[52] Huang L, Bui NN, Manickam SS, McCutcheon JR. Controlling electrospun nanofiber morphology and mechanical properties using humidity. Journal of Polymer Science Part B Polymer Physics 2011;49:1734–44.
[53] Casper CL, Stephens JS, Tassi NG, Chase DB, Rabolt JF. Controlling surface morphology of electrospun polystyrene fibers: effect of humidity and molecular weight in electrospinning process. Macromolecules 2004;37:573–88.
[54] Wang CH, Chien HS, Hsu CH, Wang YC, Wang CT, Lu HA. Electrospinning of polyacrylonitrile solutions at elevated temperatures. Macromolecules 2007;40:7973–83.
[55] Nangrejo M, Bragman F, Ahmad Z, Stride E, Edirisinghe M. Hot electrospinning of polyurethane fibres. Material Letters 2012;68:482–5.
[56] Thompson CJ, Chase GG, Yarin AL, Reneker DH. Effects of parameters on nanofiber diameter determined from electrospinning model. Polymer 2007;48:6913–22.
[57] Lin Y, Yao Y, Yang X, Wei N, Li X, Gong P, Li R, Wu D. Preparation of poly (ether sulfone) nanofibers by gas-jet electrospinning. Journal of Applied Polymer Science 2008;107:909–17.
[58] Zhmayev E, Cho D, Joo YL. Nanofibers from gas-assisted polymer melt electrospinning. Polymer 2010;51:4140–4.
[59] Wang B, Yao Y, Peng J, Lin Y, Liu W, Luo Y, Xiang R, Li R, Wu D. Preparation of poly (ester imide) ultrafine fibers by gas jet/electrospinning. Journal of Applied Polymer Science 2009;114:883–91.
[60] Wu Y, Carnell LA, Clark RL. Control of electrospun mat width through the use of parallel auxiliary electrodes. Polymer 2007;48:5653–61.
[61] Carnell LS, Siochi EJ, Holloway NM, Stephens RM, Rhim C, Niklason LE, Clark RL. Aligned mats from electrospun single fibers. Macromolecules 2008;41:5345–9.
[62] Park SA, Park K, Yoon H, Son JG, Min T, Kim GH. Apparatus for preparing electrospun nanofibers: designing an electrospinning process for nanofiber fabrication. Polymer International 2007;56:1361–6.
[63] Yang D, Lu B, Zhao Y, Jiang X. Fabrication of aligned fibrous arrays by magnetic electrospinning. Advanced Materials 2007;19:3702–6.
[64] Liu L, Zhou J, Huang X, Xiao CF. Preparation of aligned polysulfonamide nanofibers by magnetic electrospinning. Advanced Material Research 2011;332–334:363–6.
[65] Kameoka J, Orth R, Yang Y, Czaplewski D, Mathers R, Coates GW, Craighead HG. A scanning tip electrospinning source for deposition of oriented nanofibers. Nanotechnology 2003;14:1124–9.
[66] Kameoka J, Craighead HG. Fabrication of oriented polymeric nanofibers on planar surfaces by electrospinning. Applied Physics Letters 2003;83:371–3.
[67] Sun D, Chang C, Li S, Lin L. Near field electrospinning. Nano Letters 2006;6:839–42.
[68] Gururajan G, Sullivan SP, Beebe TB, Chase DB, Rabolt JF. Continuous electrospinning of polymer nanofibers of Nylon-6 using an atomic force microscope tip. Nanoscale 2011;3:3300–8.
[69] Dersch R, Graeser M, Greiner A, Wendorff JH. Electrospinning of nanofibers: Towards new techniques, functions, and applications. Australian Journal of Chemistry 2007;60:719–28.
[70] Chang CH, Limkrailassiri K, Lin L. Continuous near-field electrospinning for large area deposition of orderly nanofiber patterns. Applied Physics Letters 2008;93:123111/1–123111.
[71] Hellmann C, Belardi J, Dersch R, Greiner A, Wendorff JH, Bahnmueller S. High precision deposition electrospinning, of nanofibers and nanofiber nonwovens. Polymer 2009;50:1197–205.
[72] Brown TD, Dalton PD, Hutmacher DW. Direct writing by way of melt electrospinning. Advanced Materials 2011;23:5651–7.
[73] Pu J, Jiang YD. High efficiency electrospinning for deposition of orderly nanofibre. Material Research Innovations 2011;15: 290–3.
[74] Bisht GS, Canton G, Mirsepassi A, Kulinsky L, Oh S, Dunn-Rankin D, Madou MJ. Controlled continuous patterning of polymeric nanofibers on three-dimensional substrates using low-voltage near-field electrospinning. Nano Letters 2011;11:1831–7.
[75] Wang H, Zheng G, Li W, Wang X, Sun D. Direct-writing organic three-dimensional nanofibrous structure. Applied Physics A 2011;102:457–61.
[76] Park JU, Hardy M, Kang SJ, Barton K, Adair K, Mukhopadhyay DK, Lee CY, Strano MS, Alleyne AG, Georgiadis JG, Ferreira PM, Rogers JA. High-resolution electrodynamic jet printing. Nature Materials 2007;6:782–9.
[77] Ahmad Z, Rasekh M, Edirisinghe M. Electrohydrodynamic direct writing of biomedical polymers and composites. Macromolecular Material Engineering 2010;295:315–9.
[78] Dosunmu OO, Chase GG, Kataphinan W, Reneker DH. Electrospinning of polymer nanofibres from multiple jets on a porous tubular surface. Nanotechnology 2006;17:1123–7.
[79] Varabhas JS, Chase GG, Reneker DH. Electrospun nanofibers from a porous hollow tube. Polymer 2008;49:4226–9.
[80] Yarin AL, Zussman E. Upward needleless electrospinning of multiple nanofibers. Polymer 2004;45:2977–80.
[81] Liu Y, He JH, Xu L, Yu JY. The principle of bubble electrospinning and its experimental verification. Journal of Polymer Engineering 2008;28:55–65.
[82] Liu Y, Dong L, Fan J, Wang R, Yu JY. Effect of applied voltage on diameter and morphology of ultrafine fibers in bubble electrospinning. Journal of Applied Polymer Science 2011;120:592–8.

[83] Ren ZF, He JH. Single polymeric bubble for the preparation of multiple micro/nano fibers. Journal of Applied Polymer Science 2011;119:1161–5.
[84] Liu Y, He JH. Bubble electrospinning for mass production of nanofibers. International Journal of Nonlinear Sciences and Numerical Simulation 2007;8:393–6.
[85] Wang X, Niu H, Lin T, Wang X. Needleless electrospinning of nanofibers with a conical wire coil. Polymer Engineering & Science 2009;49:1582–6.
[86] Wang X, Xu W. Effect of experimental parameters on needleless electrospinning from a conical wire coil. Journal of Applied Polymer Science 2012;123:3703–9.
[87] Sun Z, Zussman E, Yarin AL, Wendorff JH, Greiner A. Compound core/shell polymer nanofibers by co-electrospinning. Advanced Materials 2003;15:1929–32.
[88] Yarin AL, Zussman E, Wendorff JH, Greiner A. Material encapsulation in core-shell micro/nanofibers, polymer and carbon nanotubes and micro/nanochannels. Journal of Material Chemistry 2007;17:2585–99.
[89] Yarin AL. Coaxial electrospinning and emulsion electrospinning of core–shell fibers. Polymers for Advanced Technologies 2011;22:310–7.
[90] Reznik SN, Yarin AL, Zussman E, Bercovici L. Evolution of a compound droplet attached to a core-shell nozzle under the action of a strong electric field. Physics of Fluids 2006;18:062101/1–62101.
[91] Zussman E, Yarin AL, Bazilevsky AV, Avrahami R, Feldman M. Electrospun polyaniline/poly(methyl methacrylate)-derived turbostratic carbon micro-/nanotubes. Advanced Materials 2006;18:348–53.
[92] Li D, Xia Y. Direct fabrication of composite and ceramic hollow nanofibers by electrospinning. Nano Letters 2004;4:933–8.
[93] Li D, McCann JT, Xia Y. Use of electrospinning to directly fabricate hollow nanofibers with functionalized inner and outer surfaces. Small 2005;1:83–6.
[94] Dror Y, Salalha W, Avrahami R, Zussman E, Yarin AL, Dersch R, Greiner A, Wendorff JH. One step production of polymeric microtubes by co-electrospinning. Small 2007;3:1064–73.
[95] Bazilevsky AV, Yarin AL, Megaridis CM. Co-electrospinning of core- shell fibers using a single nozzle technique. Langmuir 2007;23:2311–4.
[96] Li XH, Shao CL, Liu YC. A simple method for controllable preparation of polymer nanotubes via a single capillary electrospinning. Langmuir 2007;23:10920–3.
[97] Kim C, Jeong YI, Ngoc BTN, Yang KS, Kojima M, Kim YA, Endo M, Lee JW. Synthesis and characterization of porous carbon nanofibers with hollow cores through the thermal treatment of electrospun copolymeric nanofiber webs. Small 2007;3:91–5.
[98] Hong CK, Yang KS, Oh SH, Ahn JH, Cho BH, Nah C. Effect of blend composition on the morphology development of electrospun fibres based on PAN/PMMA blends. Polymer International 2008;57:1357–62.
[99] Zhang JF, Yang DZ, Xu F, Zhang ZP, Yin RX, Nie J. Electrospun core–shell structure nanofibers from homogeneous solution of poly(ethylene oxide)/chitosan. Macromolecules 2009;42:5278–84.
[100] Srikar R, Yarin AL, Megaridis CM, Bazilevsky AV, Kelley E. Desorption-limited mechanism of release from polymer nanofibers. Langmuir 2008;24:965–74.
[101] Bazilevsky AV, Yarin AL, Megaridis CM. Pressure-driven delivery through carbon tube bundles. Lab on a Chip 2008;8:152–60.
[102] Srikar R, Yarin AL, Megaridis CM. Fluidic delivery of homogeneous solutions through carbon tube bundles. Nanotechnology 2009;20:275706/1–275706.
[103] Sinha-Ray S, Yarin AL. Flow from macroscopically long straight carbon nanopores for generation of thermoresponsive nanoparticles. Journal of Applied Physics 2010;107:024903/1–24903.
[104] Yu DG, Branford-White C, Bligh SWA, White K, Chatterton NP, Zhu LM. Improving polymer nanofiber quality using a modified co-axial electrospinning process. Macromolecular Rapid Communications 2011;32:744–50.
[105] Yu DG, Lu P, Branford-White C, Yang JH, Wang X. Polyacrylonitrile nanofibers prepared using coaxial electrospinning with LiCl solution as sheath fluid. Nanotechnology 2011;22:435301/1–435301.
[106] Yu DG, White K, Yang JH, Wang X, Wei Q, Li Y. PVP nanofibers prepared using co-axial electrospinning with salt solution as sheath fluid. Material Letters 2012;67:78–80.
[107] Xia Y, Yang P, Sum Y, Wu Y, Mayers B, Gates B, Yin Y, Kim F, Yan H. One-dimensional nanostructures: Synthesis, characterization, and applications. Advanced Materials 2003;15:353–89.
[108] Kuo CC, Lin CH, Chen WC. Morphology and photophysical properties of light-emitting electro-spun nanofibers prepared from polyfluorene derivative/PMMA blends. Macromolecules 2007;40:6959–66.
[109] Chuangchote S, Sagawa T, Yoshikawa S. Ultrafine electrospun conducting polymer blend fibers and their photoluminescence properties. Macromolecular Symposia 2008;264:80–9.
[110] Chuangchote S, Sagawa T, Yoshikawa S. Fabrication and optical properties of electrospun conductive polymer nanofibers from blended polymer solution. Japanese Journal of Applied Physics 2008;47:787–93.
[111] Yin K, Zhang L, Lai C, Zhong L, Smith S, Fong H, Zhu Z. Photoluminescence anisotropy of uni-axially aligned electrospun conjugated polymer nanofibers of MEH-PPV and P3HT. Journal of Material Chemistry 2011;21:444–8.
[112] Pagliara S, Vitiello MS, Camposeo A, Polini A, Cingolani R, Scamarcio G, Pisignano D. Optical anisotropy in single light-emitting polymer nanofibers. Journal of Physical Chemistry C 2011;115:20399–405.
[113] Vohra V, Giovanella U, Tubino R, Murata H, Botta C. Electroluminescence from conjugated polymer electrospun nanofibers in solution processable organic light-emitting diodes. ACS Nano 2011;5:5572–8.
[114] Sui X, Shao C, Liu Y. Photoluminescence of polyethylene oxide-ZnO composite electrospun fibers. Polymer 2007;48:1459–63.
[115] Abitbol T, Wilson JT, Gray DG. Electrospinning of fluorescent fibers from CdSe/ZnS quantum dots in cellulose triacetate. Journal of Applied Polymer Science 2011;119:803–10.
[116] Benedetto FD, Camposeo A, Persano L, Laera AM, Piscopiello E, Cingolani R, Tapfer L, Pisignano D. Light-emitting nanocomposite CdS-polymer electrospun fibres via in situ nanoparticle generation. Nanoscale 2011;3:4234–9.
[117] Wang C, Yan P, Wang S, Bai X, Yuan J, Yan E, Huang Z. Novel preparation of Ag2S nanoparticles embedded in photoluminescent polymer nanofibers. Pigment & Resin Technology 2011;40:17–23.
[118] Chen J, Yang P, Wang C, Zhan S, Zhang L, Huang Z, Li W, Wang C, Jiang Z, Shao C. Ag nanoparticles/PPV composite nanofibers with high and sensitive opto-electronic response. Nanoscale Researh Letters 2011;6:121–5.
[119] Zhang H, Song H, Yu H, Bai X, Li S, Pan G, Dai Q, Wang T, Li W, Lu S, Ren X, Zhao H. Electrospinning preparation and photoluminescence properties of rare-earth complex/Polymer Composite fibers. Journal of Physical Chemistry C 2007;111:6524–7.
[120] Cui X, Zhang HM, Wu TF. Electrospinning preparation and photoluminescence properties of erbium complex doped composite fibers. Spectrochimica Acta Part A 2011;79:1998–2002.
[121] Cheng S, Li X, Xie S, Chen Y, Fan LJ. Preparation of electrospun luminescent polyimide/europium nanofibers by simultaneous in situ sol-gel and imidization processes. Journal of Colloid Interface Science 2011;356:92–9.
[122] Wang Y, Mao HJ, Zang GQ, Yu YS, Tang ZH. Photoluminescence properties of Re(I) complex doped composite submicron fibers prepared by electrospinning. Spectrochimica Acta Part A 2011;78:469–73.
[123] Bianco A, Cacciotti I, Fragalá ME, Lamastra FR, Speghini A, Piccinelli F, Malandrino G, Gusmano G. Eu-doped titania nanofibers: processing, thermal behaviour and luminescent properties. Journal of Nanoscience & Nanotechnology 2010;10:5183–90.
[124] Cacciotti I, Bianco A, Pezzotti G, Gusmano G. Synthesis, thermal behaviour and luminescence properties of rare earth-doped titania nanofibers. Chemical Engineering Journal 2011;166:751–64.
[125] Gu Y, Zhang Q, Wang H, Li Y. $CaSi_2O_2N_2$:Eu nanofiber mat based on electrospinning: facile synthesis, uniform arrangement, and application in white LEDs. Journal of Material Chemistry 2011;21:17790–7.
[126] Zhang Y, Liu Y, Li X, Wang QJ, Xie E. Room temperature enhanced red emission from novel Eu^{3+} doped ZnO nanocrystals uniformly dispersed in nanofibers. Nanotechnology 2011;22:415702/1–415702.
[127] Hou Z, Li C, Yang J, Lian H, Yang P, Chai R, Cheng Z, Lin J. One-dimensional $CaWO_4$ and $CaWO_4$:Tb^{3+} nanowires and nanotubes: elecctrospinning, preparation and luminescent properties. Journal of Material Chemistry 2009;19:2737–46.
[128] Zhao J, Zhang W, Xie E, Liu Z, Feng J, Liu Z. Photoluminescence properties of β-Ga_2O_3:Tb^{3+} nanofibers prepared by electrospinning. Material Science Engineering B 2011;176:932–6.
[129] Du P, Song L, Xiong J, Xi Z, Jin D, Wang L. Preparation and the luminescent properties of Tb^{3+}-doped Gd_2O_3 fluorescent nanofibers via electrospinning. Nanotechnology 2011;22:035602/1–35602.
[130] Cacciotti I, Bianco A, Pezzotti G, Gusmano G. Terbium and ytterbium-doped titania luminescent nanofibers by means

of electrospinning technique. Materials Chemistry & Physics 2011;126:532–41.
[131] Li X, Chen Y, Qian Q, Liu X, Xiao L, Chen Q. Preparation and photoluminescence characteristics of Tb-Sm- and Dy-doped Y_2O_3 nanofibers by electrospinning. Journal of Luminescence 2012;132:81–5.
[132] Song L, Du P, Xiong J, Fan X, Jiao Y. Preparation and luminescence properties of terbium-doped lanthanum oxide nanofibers by electrospinning. Journal of Luminescence 2012;132:171–4.
[133] Peng C, Li G, Kang X, Li C, Lin J. The fabrication of one-dimensional $Ca_4Y_6(SiO_4)_6O$: Ln^{3+} (Ln = Eu, Tb) phosphors by electrospinning method and their luminescence properties. Journal of Colloids and Interface Science 2011;355:89–95.
[134] Li X, Yu M, Hou Z, Li G, Ma P, Wang W, Cheng Z, Lin J. One-dimensional $GdVO_4$:Ln^{3+} (Ln = Eu, Dy, Sm) nanofibers: Electrospinning preparation and luminescence properties. Journal of Solid State Chemistry 2011;184:141–8.
[135] Wu J, Coffer JL. Emissive erbium-doped silicon and germanium oxide nanofibers derived from an electrospinning process. Chemistry of Materials 2007;19:6266–76.
[136] Wu J, Coffer JL. Strongly emissive erbium-doped tin oxide nanofibers derived from sol gel/electrospinning methods. Journal of Physical Chemistry C 2007;111:16088–91.
[137] Zheng R, Xu L, Qin W, Chen J, Dong B, Zhang L, Song H. Electrospinning preparation and photoluminescence properties of $SrAl_2O_4$:Ce^{3+} nanowires. Journal of Material Science 2011;46:7517–24.
[138] Kumar A, Jose R, Fujihara K, Wang J, Ramakrishna S. Structural and optical properties of electrospun TiO_2 nanofibers. Chemistry of Materials 2007;19:6536–42.
[139] Yang Y, Wang H, Lu X, Zhao Y, Li X, Wang C. Electrospinning of carbon/CdS coaxial nanofibers with photoluminescence and conductive properties. Material Science Engineering B 2007;140:48–52.
[140] Suryamas AB, Munir MM, Ogi T, Khairurrijal O, Okuyama K. Intense green and yellow emissions from electrospun BCNO phosphor nanofibers. Journal of Material Chemistry 2011;21:12629–31.
[141] Sen B, Stroscio M, Dutta M. Photoluminescence and Raman spectroscopy of polycrystalline ZnO nanofibers deposited by electrospinning. Journal of Electronic Materials 2011;40:2015–9.
[142] Barakat NAM, Al-Deyab S, Kim HY. Synthesis and study of the photoluminescence and optical characteristics of Cd/CdO nanorods prepared by the electrospinning process. Material Letters 2012;66:225–8.
[143] Andrew JS, Clarke DR. Enhanced ferroelectric phase content of polyvinylidene difluoride fibers with the addition of magnetic nanoparticles. Langmuir 2008;24:8435–8.
[144] Zhu J, Wei S, Rutman D, Haldolaarachchige N, Young DP, Guo Z. Magnetic polyacrylonitrile-Fe@FeO nanocomposite fibers—Electrospinning, stabilization and carbonization. Polymer 2011;52:2947–55.
[145] Miyauchi M, Simmons TJ, Miao J, Gagner JE, Shriver ZH, Aich U, Dordick JS, Linhardt RJ. Electrospun polyvinylpyrrolidone fibers with high concentrations of ferromagnetic and superparamagnetic nanoparticles. ACS Applied Materials & Interfaces 2011;3:1958–64.
[146] Jung JH, Hyun JYH, Park SY, Lee YP, Shin MK, Kim SJ. Giant superparamagnetic nanocomposites using ferritin. Journal of Korean Physics Society 2011;58:797–800.
[147] Graeser M, Bognitzki M, Massa W, Pietzonka C, Greiner A, Wendorff JH. Magnetically anisotropic cobalt and iron nanofibers via electrospinning. Advanced Materials 2007;19:4244–7.
[148] Wu H, Zhang R, Liu X, Lin D, Pan W. Electrospinning of Fe, Co, and Ni Nanofibers: Synthesis, assembly, and magnetic properties. Chemistry of Materials 2007;19:3506–11.
[149] Barakat NAM, Kim B, Kim HY. Production of smooth and pure nickel metal nanofibers by the electrospinning technique: nanofibers possess splendid magnetic properties. Journal of Physical Chemistry C 2009;113:531–6.
[150] Eid C, Luneau D, Salles V, Asmar R, Monteil Y, Khoury A, Brioude A. Magnetic properties of hematite nanotubes elaborated by electrospinning process. Journal of Physical Chemistry C 2011;115:17643–6.
[151] Ponhan W, Maensiri S. Fabrication and magnetic properties of electrospun copper ferrite ($CuFe_2O_4$) nanofibers. Solid State Science 2009;11:479–84.
[152] Chen X, Unruh KM, Ni C, Ali B, Sun Z, Lu Q, Deitzel J, Xiao JQ. Fabrication, formation mechanism, and magnetic properties of metal oxide nanotubes via electrospinning and thermal treatment. Journal of Physical Chemistry C 2011;11:373–8.
[153] Song JH, Nam JH, Cho JH, Kim BI, Chun MP, Choi DK. Microstructures and multiferroic properties of electrospun $BiFeO_3$ nanofibers. Journal of Korean Physics Society 2011;59:2308–12.
[154] Xie S, Ma F, Liu Y, Li J. Multiferroic $CoFe_2O_4$–$Pb(Zr_{0.52}Ti_{0.48})O_3$ core-shell nanofibers and their magnetoelectric coupling. Nanoscale 2011;3:3152–8.
[155] Shen XQ, Xiang J, Song FZ, Liu MQ. Characterization and magnetic properties of electrospun $Co_{1-x}Zn_xFe_2O_4$ nanofibers. Applied Physics A 2010;99:189–95.
[156] Arias M, Pantojas VM, Perales O, Otano W. Synthesis and characterization of magnetic diphase $ZnFe_2O_4$/γ-Fe_2O_3 electrospun fibers. The Journal of Magnetism and Magnetic Materials 2011;323:2109–14.
[157] Jalalian A, Kavrik MS, Khartsev SI, Grishin AM. Ferromagnetic resonance in $Y_3Fe_5O_{12}$ nanofibers. Applied Physics Letters 2011;99:102501/1–102501.
[158] Song F, Shen X, Liu M, Xiang J. One-dimensional $SrFe_{12}O_{19}$/$Ni_{0.5}Zn_{0.5}Fe_2O_4$ composite ferrite nanofibers and enhancement magnetic property. Journal of Nanoscience & Nanotechnology 2011;11:6979–85.
[159] Liu M, Shen X, Song F, Xiang J, Liu R. Effect of heat treatment on particle growth and magnetic properties of electrospun $S_{0.8}La_{0.2}Zn_{0.2}Fe_{11.8}O_{19}$ nanofibers. Journal of Sol-Gel Science and Technology 2011;59:553–60.
[160] Shen X, Zheng J, Meng X, Liang Q. Fabrication and magnetic properties of composite $Ni_{0.5}Zn_{0.5}Fe_2O_4$/$Pb(Zr_{0.52}Ti_{0.48})O_3$ nanofibers by electrospinning. Journal of Wuhan University of Technology—Material Science Edition 2011;26:384–7.
[161] Shen X, Liu M, Song F, Zhu Y. Effects of La-Zn substitution on microstructure and magnetic properties of strontium ferrite nanofibers. Applied Physics A 2011;104:109–16.
[162] Jugdersuren B, Kang S, DiPietro S, Heiman D, McKeown D, Pegg IL, Philip J. Large low field magnetoresistance in $La_{0.67}Sr_{0.33}MnO_3$ nanowire devices. Journal of Applied Physics 2011;109:016109/1–16109.
[163] Li CJ, Wang B, Wang JN. Magnetic and microwave absorbing properties of electrospun $Ba_{(1-x)}La_xFe_{12}O_{19}$ nanofibers. The Journal of Magnetism and Magnetic Materials 2012;324:1305–11.
[164] Li JM, Zeng XL, Wu GQ, Xu ZA. Exciton quenching and ferromagnetism-to-ferrimagnetism crossover in diluted magnetic semiconducting $Zn_{1-x}Co_xO$ nanogranular nanofibers. CrystEngComm 2012;14:525–32.
[165] Ding B, Wang M, Yu J, Sun G. Gas sensors based on electrospun nanofibers. Sensors 2009;9:1609–24.
[166] Chae SK, Park H, Yoon J, Lee CH, Ahn DJ, Kim JM. Polydiacetylene supramolecules in electrospun microfibers: fabrication, micropatterning, and sensor applications. Advanced Materials 2007;19:521–4.
[167] Manesh KM, Santhosh P, Gopalan A, Lee KP. Electrospun poly(vinylidene fluoride)/poly(aminophenylboronic acid) composite nanofibrous membrane as a novel glucose sensor. Analytical Biochemistry 2007;360:189–95.
[168] Bai H, Zhao L, Lu C, Li C, Shi G. Composite nanofibers of conducting polymers and hydrophobic insulating polymers: Preparation and sensing applications. Polymer 2009;50:3292–301.
[169] Ji L, Medford AJ, Zhang X. Electrospun polyacrylonitrile/zinc chloride composite nanofibers and their response to hydrogen sulfide. Polymer 2009;50:605–12.
[170] Jang K, Baek IW, Back SY, Ahn H. Electrospinning of porphyrin/polyvinyl alcohol (PVA) nanofibers and their acid vapor sensing capability. Journal of Nanoscience & Nanotechnology 2011;11:6102–8.
[171] Liu Z, Zhou C, Zheng B, Qian L, Mo Y, Luo F, Shi Y, Choi MMF, Xiao D. In situ synthesis of gold nanoparticles on porous polyacrylonitrile nanofibers for sensing applications. Analyst 2011;136:4545–51.
[172] Hosseinmardi A, Keyanpour-Rad M, Hesari FA. Impedance characteristics of electrospun nylon-6/TiO_2 nanocomposite for humidity sensor. Key Engineering Materials 2011;471–472:542–7.
[173] Chen D, Lei S, Chen Y. A single polyaniline nanofiber field effect transistor and its gas sensing mechanisms. Sensors 2011;11:6509–16.
[174] Li Y, Gong J, He G, Deng Y. Fabrication of polyaniline/titanium dioxide composite nanofibers for gas sensing application. Material Chemistry & Physics 2011;129:477–82.
[175] Chee PS, Arsat R, He X, Kalantar-zadeh K, Arsat M, Wlodarski W. Polyvinylpyrrolidone/multiwall carbon nanotube composite based 36° YX $LiTaO_3$ surface acoustic wave for hydrogen gas sensing applications. AIP Conference Proceedings 2011;1341:410–4.

[176] Liu S, Sun H, Nagarajan R, Kumar J, Gu Z, Cho JH, Kurup P. Dynamic chemical vapor sensing with nanofibrous film based surface acoustic wave sensors. Sensors and Actuators A 2011;167:8–13.
[177] Wang LY, Xu Y, Lin Z, Zhao N, Xu Y. Electrospinning fabrication and oxygen sensing properties of Cu(I) complex-polystyrene composite microfibrous membranes. Journal of Luminescence 2011;131:1277–82.
[178] Li Y. High performance oxygen sensing nanofibrous membranes of Eu(III) complex/polystyrene prepared by electrospinning. Spectrochimica Acta Part A 2011;79:356–60.
[179] Wang Y, Li B, Zhang L, Zuo Q, Li P, Zhang J, Su Z. High-performance oxygen sensors based on Eu(III) complex/polystyrene composite nanofibrous membranes prepared by electrospinning. ChemPhysChem 2011;12:349–55.
[180] Wang W, Huang H, Li Z, Zhang H, Wang Y, Zheng W, Wang C. Zinc oxide nanofiber gas sensors via electrospinning. Journal of the American Ceramic Society 2008;91:3817–9.
[181] Wu WY, Ting JM, Huang PJ. Electrospun ZnO nanowires as gas sensors for ethanol detection. Nanoscale Research Letters 2009;4:513–7.
[182] Feng CH, Ruan SP, Zhu LH, Li C, Li W, Chen WY, Chen LH, Zhang XD. Preparation and ethanol sensing properties of ZnO nanofibers. Chemical Research in Chinese University 2011;27:720–3.
[183] Wei S, Zhou M, Du W. Improved acetone sensing properties of ZnO hollow nanofibers by single capillary electrospinning. Sensors and Actuators B 2011;160:753–9.
[184] Choi SW, Park JY, Kim SS. Dependence of gas sensing properties in ZnO nanofibers on size and crystallinity of nanograin. Journal of Material Research 2011;26:1662–5.
[185] Lee C, Choi SW, Park JY, Kim SS. Synthesis of ZnO nanofibers and their gas sensing properties. Sensors Letters 2011;9:132–6.
[186] Horzum N, Taşçioglu D, Okur S, Demir MM. Humidity sensing properties of ZnO-based fibers by electrospinning. Talanta 2011;85:1105–11.
[187] Lee HU, Ahn K, Lee SJ, Kim JP, Kim HG, Jeong SY, Cho CR. ZnO nanobarbed fibers: Fabrication, sensing NO_2 gas, and their sensing mechanism. Applied Physics Letters 2011;98:193114/1–193114.
[188] Ahmad M, Pan C, Luo Z, Zhu J. A single ZnO nanofiber-based highly sensitive amperometric glucose biosensor. Journal of Physical Chemistry C 2010;114:9308–13.
[189] Lee BS, Kim WS, Kim DH, Kim HC, Hong SH, Yu WR. Fabrication of SnO_2 nanotube microyarn and its gas sensing behaviour. Smart Materials and Structures 2011;20:105019/1–105019.
[190] Xu X, Sun J, Zhang H, Wang Z, Dong B, Jiang T, Wang W, Li Z, Wang C. Effects of Al doping on SnO_2 nanofibers in hydrogen sensor. Sensors and Actuators B 2011;160:858–63.
[191] Cho NG, Yang DY, Jin MJ, Kim HG, Tuller HL, Kim ID. Highly sensitive SnO_2 hollow nanofiber-based NO_2 gas sensors. Sensors and Actuators B 2011;160:1468–72.
[192] Park JY, Asokan K, Choi SW, Kim SS. Growth kinetics of nanograins in SnO_2 fibers and size dependent sensing properties. Sensors and Actuators B 2011;152:254–60.
[193] Wang Y, Ramos I, Santiago-Aviles JJ. Detection of moisture and methanol gas using a single electrospun tin oxide nanofiber. IEEE Sensor Journal 2007;7:1347–8.
[194] Landau O, Rothschild A, Zussman E. Processing-microstructure-properties correlation of ultrasensitive gas sensors produced by electrospinning. Chemistry of Materials 2009;21:9–11.
[195] Park JY, Choi SW, Lee JW, Lee C, Kim SS. Synthesis and gas sensing properties of TiO_2-ZnO core-shell nanofibers. Journal of the American Ceramic Society 2009;92:2551–4.
[196] Liu L, Zhong Z, Wang Z, Wang L, Li S, Liu Z, Han Y, Tian Y, Wu P, Meng X. Synthesis, characterization, and m-xylene sensing properties of Co-ZnO composite nanofibers. Journal of the American Ceramic Society 2011;94:3437–41.
[197] Yue XJ, Hong TS, Xu X, Li Z. High-performance humidity sensors based on double-layer ZnO-TiO_2 nanofibers via electrospinning. Chinese Physics Letters 2011;28:090701/1–90701.
[198] Xu L, Wang R, Xiao Q, Zhang D, Liu Y. Micro humidity sensor with high sensitivity and quick response/recovery based on ZnO/TiO_2 composite nanofibers. Chinese Physics Letters 2011;28:070702/1–70702.
[199] Park JY, Choi SW, Kim SS. A model for the enhancement of gas sensing properties in SnO_2-ZnO core-shell nanofibres. Journal of Physics D 2011;44:205403/1–205403.
[200] Wei S, Zhang Y, Zhou M. Toluene sensing properties of SnO_2-ZnO hollow nanofibers fabricated from single capillary electrospinning. Solid State Communications 2011;151:895–9.
[201] Zhao M, Wang X, Ning L, Jia J, Li X, Cao L. Electrospun Cu-doped ZnO nanofibers for H_2S sensing. Sensors and Actuators B 2011;156:588–92.
[202] Khorami HA, Keyanpour-Rad M, Vaezi MR. Synthesis of SnO_2/ZnO composite nanofibers by electrospinning method and study of its ethanol sensing properties. Applied Surface Sciences 2011;257:7988–92.
[203] Wang Z, Liu L. Synthesis and ethanol sensing properties of Fe-doped SnO_2 nanofibers. Material Letters 2009;63:917–9.
[204] Yang DJ, Kamienchick I, Youn DY, Rothschild A, Kim ID. Ultrasensitive and highly selective gas sensors based on electrospun SnO_2 nanofibers modified by Pd loading. Advanced Functional Material 2010;20:4258–64.
[205] Dong KY, Choi JK, Hwang IS, Lee JW, Kang BH, Ham DJ, Lee JH, Ju BK. Enhanced H_2S sensing characteristics of Pt doped SnO_2 nanofibers sensors with micro heater. Sensors and Actuators B 2011;157:154–61.
[206] Zheng Y, Wang J, Yao P. Formaldehyde sensing properties of electrospun NiO-doped SnO_2 nanofibers. Sensors and Actuators B 2011;156:723–30.
[207] Wang Y, Jia W, Strout T, Schempf A, Zhang H, Li B, Cui J, Lei Y. Ammonia gas sensor using polypyrrole-coated TiO_2/ZnO nanofibers. Electroanalysis 2009;21:1432–8.
[208] Ding Y, Wang Y, Zhang L, Zhang H, Li CM, Lei Y. Preparation of TiO_2-Pt hybrid nanofibers and their application for sensitive hydrazine detection. Nanoscale 2011;3:1149–57.
[209] He X, Zhao Y, Li J, Gao X, Jia J. Porous CuO electrospun fibers and their gas sensing properties. Sensor Letters 2011;9:294–8.
[210] Wang W, Zhang L, Tong S, Li X, Song W. Three-dimensional network films of electrospun copper oxide nanofibers for glucose determination. Biosensors & Bioelectronics 2009;25:708–14.
[211] Choi SW, Park JY, Kim SS. Growth behavior and sensing properties of nanograins in CuO nanofibers. Chemical Engineering Journal 2011;172:550–6.
[212] Wang W, Li Z, Zheng W, Yang J, Zhang H, Wang C. Electrospun palladium (IV)-doped copper oxide composite nanofibers for non-enzymatic glucose sensors. Electrochemical Communications 2009;11:1811–4.
[213] Wang Y, Wang W, Song W. Binary CuO/Co_3O_4 nanofibers for ultrafast and amplified electrochemical sensing of fructose. Electrochimica Acta 2011;56:10191–6.
[214] Zheng W, Li Z, Zhang H, Wang W, Wang Y, Wang C. Electrospinning route for α-Fe_2O_3 ceramic nanofibers and their gas sensing properties. Material Research Bulletin 2009;44:1432–6.
[215] Fan H, Zhang T, Xu X, Lv N. Fabrication of N-type Fe_2O_3 and P-type $LaFeO_3$ nanobelts by electrospinning and determination of gas-sensing properties. Sensors and Actuators B 2011;153:83–8.
[216] Huang S, Ding Y, Liu Y, Su L, Filosa R, Lei Y. Glucose biosensor using glucose oxidase and electrospun Mn_2O_3-Ag nanofibers. Electroanalysis 2011;23:1912–20.
[217] Ding Y, Hou C, Li B, Lei Y. Sensitive hydrazine detection using a porous Mn_2O_3 nanofibers-based sensor. Electroanalysis 2011;23:1245–51.
[218] He Y, Liu X, Wang R, Zhang T. An excellent humidity sensor with rapid response based on $BaTiO_3$ nanofiber via electrospinning. Sensor Letters 2011;9:262–5.
[219] Wang L, He Y, Hu J, Qi Q, Zhang T. DC humidity sensing properties of $BaTiO_3$ nanofiber sensors with different electrode materials. Sensors and Actuators B 2011;153:460–4.
[220] Liu Y, Teng H, Hou H, You T. Nonenzymatic glucose sensor based on renewable electrospun Ni nanoparticle-loaded carbon nanofiber paste electrode. Biosensors & Bioelectronics 2009;24:3329–34.
[221] Ding Y, Liu Y, Parisi J, Zhang L, Lei Y. A novel NiO-Au hybrid nanobelts based sensor for sensitive and selective glucose detection. Biosensors & Bioelectronics 2011;28:393–8.
[222] Huang J, Liu Y, Hou H, You T. Simultaneous electrochemical determination of dopamine, uric acid and ascorbic acid using palladium nanoparticle-loaded carbon nanofibers modified electrode. Biosensors & Bioelectronics 2008;24:632–7.
[223] Liu Y, Huang J, Hou H, You T. Simultaneous determination of dopamine, ascorbic acid and uric acid with electrospun carbon nanofibers modified electrode. Electrochemistry Communications 2008;10:1431–4.
[224] Xu X, Fan H, Liu Y, Wang L, Zhang T. Au-loaded In_2O_3 nanofibers-based ethanol micro gas sensor with low power consumption. Sensors and Actuators B 2011;160:713–9.
[225] Nguyen TA, Park S, Kim JB, Kim TK, Seong GH, Choo J, Kim YS. Polycrystalline tungsten oxide nanofibers for gas-sensing applications. Sensors and Actuators B 2011;160:549–54.

[226] Choi SH, Hwang IS, Lee JH, Oh SG, Kim ID. Microstructural control and selective C_2H_5OH sensing properties of Zn_2SnO_4 nanofibers prepared by electrospinning. Chemistry Communications 2011;47:9315–7.
[227] Hu L, Li Y. Improved acetone sensing properties of flat sensors based on Co-SnO_2 composite nanofibers. Chinese Science Bulletin 2011;56:2644–8.
[228] Fan HT, Xu XJ, Ma XK, Zhang T. Preparation of $LaFeO_3$ nanofibers by electrospinning for gas sensors with fast response and recovery. Nanotechnology 2011;22:115502/1–115502.
[229] Leng JY, Xu XJ, Lv N, Fan HT, Zhang T. Synthesis and gas-sensing characteristics of WO_3 nanofibers via electrospinning. Journal of Colloid & Interface Science 2011;356:54–7.
[230] Marx S, Jose MV, Andersen JD, Russell AJ. Electrospun gold nanofiber electrodes for biosensors. Biosensors & Bioelectronics 2011;26:2981–6.
[231] Wang L, Yu Y, Chen PC, Chen CH. Electrospun carbon-cobalt composite nanofiber as an anode material for lithium ion batteries. Scripta Materialia 2008;58:405–8.
[232] Fan Q, Whittingham MS. Electrospun manganese oxide nanofibers as anodes for lithium-ion batteries. Electrochemical & Solid-State Letters 2007;10:A48–51.
[233] Ji L, Lin Z, Guo B, Medford AJ, Zhang X. Assembly of carbon-SnO_2 core-sheath composite nanofibers for superior lithium storage. Chemistry—A European Journal 2010;16:11543–8.
[234] Li L, Yin X, Liu S, Wang Y, Chen L, Wang T. Electrospun porous SnO_2 nanotubes as high capacity anode materials for lithium ion batteries. Electrochemistry Communications 2010;12:1383–6.
[235] Yu Y, Yang Q, Teng D, Yang X, Ryu S. Reticular Sn nanoparticle-dispersed PAN-based carbon nanofibers for anode material in rechargeable lithium-ion batteries. Electrochemistry Communications 2010;12:1187–90.
[236] Han H, Song T, Bae JY, Nazar LF, Kim H, Paik U. Nitridated TiO_2 hollow nanofibers as an anode material for high power lithium ion batteries. Energy & Environmental Science 2011;4:4532–6.
[237] Wang H, Gao P, Lu S, Liu H, Yang G, Pinto J, Jiang X. The effect of tin content to the morphology of Sn/carbon nanofiber and the electrochemical performance as anode material for lithium batteries. Electrochimica Acta 2011;58:44–51.
[238] Yuan T, Zhao B, Cai R, Zhou Y, Shao Z. Electrospinning based fabrication and performance improvement of film electrodes for lithium-ion batteries composed of TiO_2 hollow fibers. Journal of Material Chemistry 2011;21:15041–8.
[239] Wang L, Wu L, Li Z, Lei G, Xiao Q, Zhang P. Synthesis and electrochemical properties of $Li_2ZnTi_3O_8$ fibers as an anode material for lithium-ion batteries. Electrochimica Acta 2011;56:5343–6.
[240] Toprakci O, Ji L, Lin Z, Toprakci HAK, Zhang X. Fabrication and electrochemical characteristics of electrospun $LiFePO_4$/carbon composite fibers for lithium-ion batteries. Journal of Power Sources 2011;196:7692–9.
[241] Bonino CA, Ji L, Lin Z, Toprakci O, Zhang X, Khan SA. Electrospun carbon-tin oxide composite nanofibers for use as lithium ion battery anodes. ACS Applied Materials & Interfaces 2011;3:2534–42.
[242] Kong J, Liu Z, Yang Z, Tan HR, Xiong S, Wong SY, Li X, Lu X. Carbon/SnO_2/carbon core/shell/shell hybrid nanofibers: tailored nanostructure for the anode of lithium ion batteries with high reversibility and rate capacity. Nanoscale 2012;4:525–30.
[243] Lee BS, Son SB, Park KM, Yu WR, Oh KH, Lee SH. Anodic properties of hollow carbon nanofibers for Li-ion battery. Journal of Power Sources 2012;199:53–60.
[244] Mai L, Xu L, Han C, Xu X, Luo Y, Zhao S, Zhao Y. Electrospun ultralong hierarchical vanadium oxide nanowires with high performance for lithium ion batteries. Nano Letters 2010;10:4750–5.
[245] Cheah YL, Gupta N, Pramana SS, Aravindan V, Wee G, Srinivasan M. Morphology, structure and electrochemical properties of single phase electrospun vanadium pentoxide nanofibers for lithium ion batteries. Journal of Power Sources 2011;196:6465–72.
[246] Yu D, Chen C, Xie S, Liu Y, Park K, Zhou X, Zhang Q, Li J, Cao G. Mesoporous vanadium pentoxide nanofibers with significantly enhanced Li-ion storage properties by electrospinning. Energy & Environmental Science 2011;4:858–61.
[247] Kim JK, Cheruvally G, Choi JW, Ahn JH, Choi DS, Song CE. Rechargeable organic radical battery with electrospun, fibrous membrane-based polymer electrolyte. Journal of Electrochemical Society 2007;154:A839–43.
[248] Li X, Cheruvally G, Kim JK, Choi JW, Ahn JH, Kim KW, Ahn JH. Polymer electrolytes based on an electrospun poly(vinylidene fluoride-co-hexafluoropropylene) membrane for lithium batteries. Journal of Power Sources 2007;167:491–8.
[249] Raghavan P, Choi JW, Ahn JH, Cheruvally G, Chauhan GS, Ahn HJ, Nah C. Novel electrospun poly(vinylidene fluoride-co-hexafluoropropylene)-in situ SiO_2 composite membrane-based polymer electrolyte for lithium batteries. Journal of Power Sources 2008;184:437–43.
[250] Kim JK, Cheruvally G, Li X, Ahn JH, Kim KW, Ahn HJ. Preparation and electrochemical characterization of electrospun, microporous membrane-based composite polymer electrolytes for lithium batteries. Journal of Power Sources 2008;178:815–20.
[251] Cho TH, Sakai T, Tanase S, Kimura K, Kondo Y, Tarao T, Tanaka M. Electrochemical performances of polyacrylonitrile nanofiber-based nonwoven separator for lithium-ion battery. Electrochemical & Solid-State Letters 2007;10:A159–62.
[252] Carol P, Ramakrishnan P, John B, Cheruvally G. Preparation and characterization of electrospun poly(acrylonitrile) fibrous membrane based gel polymer electrolytes for lithium-ion batteries. Journal of Power Sources 2011;196:10156–62.
[253] Raghavan P, Manuel J, Zhao X, Kim DS, Ahn JH, Nah C. Preparation and electrochemical characterization of gel polymer electrolyte based on electrospun polyacrylonitrile nonwoven membranes for lithium batteries. Journal of Power Sources 2011;196:6742–9.
[254] Liang Y, Lin Z, Qiu Y, Zhang X. Fabrication and characterization of LATP/PAN composite fiber-based lithium-ion battery separators. Electrochimica Acta 2011;56:6474–80.
[255] Liang Y, Ji L, Guo B, Lin Z, Yao Y, Li Y, Alcoutlabi M, Qiu Y, Zhang X. Preparation and electrochemical characterization of ionic-conducting lithium lanthanum titanate oxide/polyacrylonitrile submicron composite fiber-based lithium-ion battery separators. Journal of Power Sources 2011;196:436–41.
[256] Hwang K, Kwon B, Byun H. Preparation of PVdF nanofiber membranes by electrospinning and their use as secondary battery separators. Journal of Membrane Science 2011;378:111–6.
[257] Zhong Z, Cao Q, Jing B, Wang X, Li X, Deng H. Electrospun PVDF-PVC nanofibrous polymer electrolytes for polymer lithium-ion batteries. Material Science Engineering B 2012;177:86–91.
[258] Wu N, Cao Q, Wang X, Li X, Deng H. A novel high-performance gel polymer electrolyte membrane basing on electrospinning technique for lithium rechargeable batteries. Journal of Power Sources 2011;196:8638–43.
[259] Ballengee JB, Pintauro PN. Composite fuel cell membranes from dual-nanofiber electrospun mats. Macromolecules 2011;44:7307–14.
[260] Shabani I, Hasani-Sadrabadi MM, Haddadi-Asl V, Soleimani M. Nanofiber-based polyelectrolytes as novel membranes for fuel cell applications. Journal of Membrane Science 2011;368:233–40.
[261] Yao Y, Ji L, Lin Z, Li Y, Alcoutlabi M, Hamouda H, Zhang X. Sulfonated polystyrene fiber network-induced hybrid proton exchange membranes. ACS Applied Materials & Interfaces 2011;3:3732–7.
[262] Mollá S, Compan V. Polyvinyl alcohol nanofiber reinforced Nafion membranes for fuel cell applications. Journal of Membrane Science 2011:372191–200.
[263] Mollá S, Compan V. Performance of composite Nafion/PVA membranes for direct methanol fuel cells. Journal of Power Sources 2011;196:2699–708.
[264] Yao Y, Lin Z, Li Y, Alcoutlabi M, Hamouda H, Zhang X. Superacidic electrospun fiber-Nafion hybrid proton exchange membranes. Advanced Energy Materials 2011;1:1133–40.
[265] Chou CC, Huang CF, Chen MJ. Fabrication and characterization of solid oxide fuel cell anode with impregnated catalytic Ni-CeO2 nano-particles on 8YSZ fibers. Advanced Materials Research 2011;287–290:2485–8.
[266] Li L, Zhang P, Liu R, Guo SM. Preparation of fibrous Ni-coated-YSZ anodes for solid oxide fuel cells. Journal of Power Sources 2011;196:1242–7.
[267] Zhi M, Mariani N, Gerdes K, Wu N. Nanofiber scaffold for solid oxide fuel cell cathode. ECS Transactions 2011;35:2201–7.
[268] Shahgaldi S, Yaakob Z, Khadem DJ, Daud WRW. Synthesize and evaluation of electrospun perovskite ($Ba_{0.5}Sr_{0.5}Co_{0.2}Fe_{0.8}O_{3-\delta}$) nanofibers for intermediate temperature solid-oxide fuel cell. Applied Mechanics & Materials 2011;52–54:1544–50.
[269] Pan C, Wu H, Wang C, Wang B, Zhang L, Cheng Z, Hu P, Pan W, Zhou Z, Yang X, Zhu Z. Nanowire-based high-performance "micro fuel cells": one nanowire, one fuel cell. Advanced Materials 2008;20:1644–8.
[270] Chen S, Hou H, Harnisch F, Patil SA, Carmona-Martinez AA, Agarwal S, Zhang Y, Sinha-Ray S, Yarin AL, Greiner A, Schröder U. Electrospun and solution blown three-dimensional carbon fiber nonwovens for application as electrodes in microbial fuel cells. Energy & Environmental Science 2011;4:1417–21.

[271] Lee BH, Song MY, Jang SY, Jo SM, Kwak SY, Kim DY. Charge transport characteristics of high efficiency dye-sensitized solar cells based on electrospun TiO_2 nanorod photoelectrodes. Journal of Physical Chemistry C 2009;113:21453–7.
[272] Zhang W, Zhu R, Liu B, Ramakrishna S. Low-cost fabrication of TiO_2 nanorod photoelectrode for dye-sensitized solar cell application. Australian Journal of Chemistry 2011;64:1282–7.
[273] Francis L, Nair AS, Jose R, Ramakrishna S, Thavasi V, Marsano E. Fabrication and characterization of dye-sensitized solar cells from rutile nanofibers and nanorods. Energy 2011;36:627–32.
[274] Joshi P, Zhang L, Davoux D, Zhu Z, Galipeau D, Fong H, Qiao Q. Composite of TiO_2 nanofibers and nanoparticles for dye-sensitized solar cells with significantly improved efficiency. Energy & Environmental Science 2010;3:1507–10.
[275] Zhang W, Zhu R, Ke L, Liu X, Liu B, Ramakrishna S. Anatase mesoporous TiO_2 nanofibers with high surface area for solid-state dye-sensitized solar cells. Small 2011;6:2176–82.
[276] Nair AS, Jose R, Shengyuan S, Ramakrishna S. A simple recipe for an efficient TiO_2 nanofiber-based dye-sensitized solar cell. Journal of Colloid Interface Science 2010;353:39–45.
[277] Krishnamoorthy T, Thavasi V, Mhaisalkar SG, Ramakrishna S. A first report on the fabrication of vertically aligned anatase TiO_2 nanowires by electrospinning preferred architecture for nanostructured solar cells. Energy & Environmental Science 2011;4:2807–12.
[278] Sudhagar P, Jung JH, Park S, Lee YG, Sathyamoorthy R, Kang YS, Ahn H. The performance of coupled (CdS:CdSe) quantum dot-sensitized TiO_2 nanofibrous solar cells. Electrochemistry Communications 2009;11:2220–4.
[279] Li J, Chen X, Ai N, Hao J, Chen Q, Strauf S, Shi Y. Silver nanoparticle doped TiO_2 nanofiber dye sensitized solar cells. Chemical Physics Letters 2011;514:141–5.
[280] Yang L, Leung WWF. Application of a bilayer TiO_2 nanofiber photoanode for optimization of dye-sensitized solar cells. Advanced Materials 2011;23:4559–62.
[281] Park SH, Choi HJ, Lee SB, Lee SM, Cho SE, Kim KH, Kim YK, Kim MR, Lee JK. Fabrications and photovoltaic properties of dye-sensitized solar cells with electrospun poly(vinyl alcohol) nanofibers containing Ag nanoparticles. Macromolecular Research 2011;19:142–6.
[282] Yun S, Lim S. Improved conversion efficiency in dye-sensitized solar cells based on electrospun Al-doped ZnO nanofiber electrodes prepared by seed layer treatment. Journal of Solid State Chemistry 2011;184:273–9.
[283] Kumar EN, Jose R, Archana PS, Vijila C, Yusoff MM, Ramakrishna S. High performance dye-sensitized solar cells with record open circuit voltage using tin oxide nanoflowers developed by electrospinning. Energy & Environmental Science 2012;5:5401–7.
[284] Joshi P, Zhang L, Chen Q, Galipeau D, Fong H, Qiao Q. Electrospun carbon nanofibers as low-cost counter electrode for dye-sensitized solar cells. ACS Applied Materials & Interfaces 2010;2:3572–7.
[285] Chuangchote S, Jitputti J, Sagawa T, Yoshikawa S. Photocatalytic activity for hydrogen evolution of electrospun TiO_2 nanofibers. ACS Applied Materials & Interfaces 2009;1:1140–3.
[286] Li D, Xia Y. Fabrication of titania nanofibers by electrospinning. Nano Letters 2003;3:555–60.
[287] He T, Zhou Z, Xu W, Ren F, Ma H, Wang J. Preparation and photocatalysis of TiO_2–fluoropolymer electrospun fiber nanocomposites. Polymer 2009;50:3031–6.
[288] Zhang X, Xu S, Han G. Fabrication and photocatalytic activity of TiO_2 nanofiber membrane. Material Letters 2009;63:1761–3.
[289] Hamadanian M, Akbari A, Jabbari V. Electrospun titanium dioxide nanofibers: fabrication, properties and its application in photooxidative degradation of methyl orange (MO). Fibers & Polymers 2011;12:880–5.
[290] Meng X, Shin DW, Yu SM, Jung JH, Kim HI, Lee HM, Han YH, Bhoraskar V, Yoo JB. Growth of hierarchical TiO_2 nanostructures on anatase nanofiibers and their application in photocatalytic activity. CrystEngComm 2011;13:3021–9.
[291] Pan C, Dong L, Gu ZZ. Surface functionalization of electrospun TiO_2 nanofibers by Au sputter coating for photocatalytic applications. International Journal of Applied Ceramic Technology 2010;7:895–900.
[292] Mishra S, Ahrenkiel SP. Synthesis and characterization of electrospun nanocomposite TiO_2 nanofibers with Ag nanoparticles for photocatalysis applications. Journal of Nanomaterials 2012:902491/1–902491.
[293] Formo E, Lee E, Campbell D, Xia Y. Functionalization of electrospun TiO_2 nanofibers with Pt nanoparticles and nanowires for catalytic applications. Nano Letters 2008;8:668–72.
[294] Wang Y, Su YR, Qiao L, Liu LX, Su Q, Zhu CQ, Liu XQ. Synthesis of one-dimensional TiO_2/V_2O_5 branched heterostructures and their visible light photocatalytic activity towards Rhodamine B. Nanotechnology 2011;22:225702/1–225702.
[295] Nakata K, Liu B, Goto Y, Ochiai T, Sakai M, Sakai H, et al. Visible light responsive electrospun TiO_2 fibers embedded with WO_3 nanoparticles. Chemistry Letters 2011;40:1161–2.
[296] Hu G, Meng X, Feng X, Ding Y, Zhang S, Yang M. Anatase TiO_2 nanoparticles/carbon nanotubes nanofibers: preparation, characterization and photocatalytic properties. Journal of Material Science 2007;42:7162–70.
[297] Liu Z, Sun DD, Guo P, Leckie JO. An efficient bicomponent TiO_2/SnO_2 nanofiber photocatalyst fabricated by electrospinning with a side-by-side dual spinneret method. Nano Letters 2007;7:1081–5.
[298] Wang C, Shao C, Liu Y, Zhang L. Photocatalytic properties BiOCl and Bi_2O_3 nanofibers prepared by electrospinning. Scripta Materialia 2008;59:332–5.
[299] Wang R, Guo J, Chen D, Miao YE, Pan J, Tjiu WW, Liu T. "Tube brush" like ZnO/SiO_2 hybrid to construct a flexible membrane with enhanced photocatalytic properties and recycling ability. Journal of Material Chemistry 2011;21:19375–80.
[300] Pan C, Dong L, Qu B, Wang J. Facile synthesis and enhanced photocatalytic performance of 3D ZnO hierarchical structures. Journal of Nanoscience & Nanotechnology 2011;11:5042–8.